The Dissertation Committee for Sanjoy Kumar Saha Certifies that this is the approved version of the following dissertation:

Theoretical Study of Thermal Transport at Nano Constrictions and Nanowires with Sawtooth Surface Roughness

Committee:

Li Shi, Supervisor

Ofodike A. Ezekoye

John R. Howell

Gyeong S. Hwang

Uttam Ghoshal

Theoretical Study of Thermal Transport at Nano Constrictions and Nanowires with Sawtooth Surface Roughness

by

Sanjoy Kumar Saha, B. Tech.; M.S.

Dissertation

Presented to the Faculty of the Graduate School of

The University of Texas at Austin

in Partial Fulfillment

of the Requirements

for the Degree of

Doctor of Philosophy

The University of Texas at Austin

May, 2007

Dedicated to my wife Tania

Acknowledgements

I am deeply indebted to my advisor, Professor Li Shi, for his constant support. Without his help, this work would never be done. I am thankful to members of my PhD advisory committee who attended my defense: Professor O. A. Ezekoye, Professor J. R. Howell, Professor G. S. Hwang and Dr. U. Ghoshal. I would like to specially thank Dr. Ravi Prasher for guiding me. I would like to mention many friends around the campus who have helped me: Arden Moore, Jae Hun Seol, Anastassios Mavrokefalos, Jianhua Zhou, Choongho Yu and others. I would like to thank my wife Tania for endless love, sacrifice and encouragement.

Theoretical Study of Thermal Transport at Nano Constrictions and Nanowires with Sawtooth Surface Roughness

Publication No._____

Sanjoy Kumar Saha, Ph.D.

The University of Texas at Austin, 2007

Supervisor: Li Shi

This dissertation is focused on thermal transport at nanometer scale point and line constrictions and in nanowires with sawtooth surface roughness. To better understand thermal transport at a point contact such as that at the tip-sample junction of a scanning probe microscope, a Non Equilibrium Molecular Dynamics (NEMD) method is employed to calculate the temperature distribution and thermal resistance of a nanoscale point constriction formed between two silicon substrates. The simulation reveals surface reconstruction at the two free silicon surfaces and at the constriction. The radius of the heated zone in the cold substrate approaches a limit of about 20 times the average nearest-neighbor distance of boron doping atoms when the constriction radius (a) is reduced below the inter-dopant distance. The phonon mean free path at the constriction is suppressed by diffuse phonon-surface scattering and phonon-impurity scattering. The MD thermal resistance is close to the ballistic resistance when a is larger than 1 nm, suggesting that surface reconstruction does not reduce the phonon transmission

coefficient significantly. When a is 0.5 nm and comparable to the dominant phonon wavelength, however, the NEMD result is considerably lower than the calculated ballistic resistance because bulk phonon dispersion and bulk potential are not longer accurate. The MD thermal resistance of the constriction increases slightly with increasing doping concentration due to the increase in the diffusive resistance.

The NEMD method is further employed to calculate the temperature distribution and thermal resistance at nanoscale line constrictions formed between two silicone substrates. Similar to the nano point constriction, the thermal resistance at the nano line constriction is dominated by the ballistic resistance for constriction width in the range of 1 nm to 12 nm.

An additional question that this dissertation seeks to answer is whether one can engineer the surface roughness on a nanowire to facilitate phonon backscattering so as to reduce the thermal conductivity below the diffuse surface limit. Monte Carlo simulation is used to show that phonon backscattering can occur at sawtooth surfaces of a silicon nanowire, suppressing the thermal conductivity below the diffuse surface limit. Asymmetric sawtooth nanowire surfaces can further cause phonon rectification, making the axial thermal conductance of the nanowire direction dependent. The phonon backscattering and rectification effects can be employed to enhance the thermoelectric figure of merit of nanowires.

Table of Contents

List of Tables

List of Figures

Chapter 1 Introduction

Dramatic technological advances in the past three decades have enabled the creation of structures with characteristic sizes smaller than 100 nm. Behavior of nanostructures is radically different from that of larger structures. As dimensions decrease, volumetric forces become negligible, quantum mechanical effects become pronounced, and boundaries and interfaces more strongly influence energy transport. The changes induced by shrinking dimensions to the nanoscale can be harnessed to build fundamentally new types of devices or to custom engineer, at the atomic scale, artificial materials with properties not found in nature.

Thermal management is widely recognized to be an important aspect of these nanostructures and nanodevices, with the device performance being significantly affected by temperature. In addition, the device lifetime can be decreased drastically because of large thermal stresses that occur especially at interfaces. The ability of a structure to remove heat is best quantified by its thermal resistance, which is given by the temperature difference divided by input power. In microprocessor design, the allowable temperature drop between the transistor (where most of the heat is generated) and the ambient air is constant. As a result, the challenge for thermal management is to develop high-conductivity structures that can accommodate this fixed temperature drop with the increasing power densities that characterize new generations of microprocessors. When the characteristic size of the material is reduced below the mean free path of the energy carriers, thermal conductivity reduces below the bulk values, exacerbating the problem of heat dissipation. Thermal contact resistance plays a significant role in these nanostructure

devices, where the contact length scale between these devices and substrate can be as small as on the order of nanometers. A solid understanding of thermal transport in these nanoscale constrictions is critical to optimize the performance of these devices.

1.1 NANOSCALE THERMAL SIMULATION APPROACHES

An accurate numerical prediction of the thermal transport in nanoscale crystalline structures is very important for both fundamental physics and engineering applications. A comprehensive analysis of thermal conductivities of nanostructures can lead to a deeper understanding of phonon scattering mechanisms, which is of fundamental theoretical significance. In addition, aggressive miniaturization of micro-electronic devices leads to substantially increased power dissipation. Thermal management is problematic in such devices because at the sub 100 nm characteristic length scales, thermal conductivity deviates significantly from bulk values and accurate values are often not known. A large number of studies report the thermal characteristics of bulk and microscale crystalline structures using both theoretical analysis and experimental techniques. The thermal energy in semiconductors such as silicon is mainly transported by phonons (Ashcroft and Mermin 1976), i.e. the quanta of lattice vibration. Boltzmann Transport Equation (BTE) governs the transport and interaction among phonons (Holland 1963). The BTE describes the phonon's transport by means of a diffusive term and the phonon's interaction by means of a scattering term. The integral-differentia1 scattering term is commonly modeled by means of the relaxation time approximation (Ziman 1960; Narumanchi, Murthy et al. 2003; Narumanchi, Murthy et al. 2004). In this approximation, the scattering term is taken to be proportional to the difference between the phonons'

equilibrium distribution for the given temperature divided by the actual distribution to the average time required to reach equilibrium, i.e. the relaxation time. Models describing the interactions (scattering) among phonons have been developed (Klemens 1958; Han and Klemens 1993; Tamura, Tanaka et al. 1999). Additionally, models have been developed to account for the scattering between phonons and vacancies/impurities/isotopes (Klemens 1958; Balandin 1998; Tamura, Tanaka et al. 1999). It is through the relaxation time that the models developed for the different scattering mechanism enter the BTE. Finally, the scattering models have been validated via predictions of bulk silicon thermal conductivity at different temperatures (Holland 1963; Narumanchi 2003). These studies assume that the phonon properties (dispersion relation and relaxation time) are isotropic and equal to the phonon properties in the [l00] crystallographic direction of silicon. More recent BTE-based numerical approaches (Narumanchi, Murthy et al. 2004) incorporate the phonon-phonon scattering mechanisms by using individual scattering terms for each possible phonon-phonon scattering mechanism. The individual scattering terms are simplified by the relaxation time approximation, where the phonon-phonon relaxation times are computed using perturbation theory (Klemens 1958; Han and Klemens 1993). This approach is also validated by predicting the bulk silicon thermal conductivity, where the Griineisen parameter is used as the tuning parameter (Narumanchi, Murthy et al. 2004). BTE based approach offer a tremendous potential to model thermal transport. However, since many assumptions must be introduced to reach a closed form solution, the results usually deviate significantly from experimental observations. To predict bulk silicon thermal conductivity, BTE is solved at a time scale and length scales much larger than the phonons' relaxation time and mean free path, respectively. Different

mathematical expressions can be used for these quantities and still reproduce the bulk silicon thermal conductivity over the solid-state temperature span (Chung, McGaughey et al. 2004). Studies towards the numerical prediction of the relaxation times (McGaughey and Kaviany 2004) and phonon scattering rules (Sinha, Schelling et al. 2003) have been performed.

Another method to simulate phonon transport properties is Molecular Dynamics (MD). MD (Allen and Tildesley 1987; Rapaport 2004) is a computation technique that simulates the behavior of materials and calculates their physical properties by solving the simultaneous equations of motions for a system of atoms interacting with a given potential. The field of MD has grown considerably due to monumental advances in computer speed and memory over the past two decades. In 1950s, MD simulation was first applied to calculate the inharmonic one-dimensional chains of atoms (Fermi et al., 1965). Early work of MD simulation has been carried out by Alder et al. (1960), Gibson et al. (1960), and Rahrnan (1964). The MD technique has been applied to liquids and gases to give reasonable results (Allen and Tildesley, 1987; Evans and Morris, 1990; Lee et al., 1991) and determine the phonon spectra and nanoscale solid structure (Hakim and Glyde, 1990; Meyer and Entel, 1998; Wang et al., 1990). Work has also been done for studying the thermal conductivity of materials (Ladd, 1986; Volz et al., 1996). Recently, Lukes et al. (1998) used MD simulation to study the thermal conductivity of solid thin films, showing that the thermal conductivity decreased as film thickness was reduced. Using MD simulation, Volz and Chen (1999) investigated the thermal conductivity of silicon nanowires and found that the simulated thermal conductivity was about two orders of magnitude smaller than that of bulk silicon crystals. They also studied the thermal

conductivity of silicon crystals and the effect of the domain size and boundary conditions (Volz and Chen, 2000).

A key advantage of MD is that it easily models materials with imperfections, interfaces, and irregularities due to the fact that it builds each structure atom by atom. This allows the construction and analyses of thin films, nanowires, carbon nanotubes, quantum dots, etc. Another advantage of MD is its conceptual simplicity and fundamental nature. The physical properties it calculates come directly from analysis of the position, velocities and forces acting on the atoms, whose atoms are governed only by the intermolecular potential specified in the simulation. Unlike other computational approaches, molecular dynamics simulations of thermal conduction do not explicitly model phonon motion nor utilize higher-level constructs such as relaxation times and scattering mechanisms. Rather all information derives from physical atom-atom interactions. A third benefit is the ability of MD to access extreme temperatures and pressure that are difficult or impossible to explore using experimental or analytical models.

The primary drawback of MD is that its computationally intensive nature limits its applicability. Full first-principles quantum mechanical calculations provide the best description of behavior at small length scales but become computationally challenging beyond few tens of atoms. Using classical intermolecular potential models allows the treatment of significantly larger number of atoms.

Different methods have been developed to calculate thermal conductivities using MD. The non-equilibrium molecular dynamics (NEMD) method consists of artificially imposing either a temperature gradient or a heat flux (Miiller-Plathe 1997; Jund and

Jullien 1999; Lukes, Li et al. 2000; Daly and Maris 2002; Schelling, Phillpot et al. 2002) in a specific direction and computing the thermal conductivity in this direction by means of Fourier's law. The equilibrium molecular dynamics (EMD) method uses the Green-Kubo relation (McQuarrie 1976; Allen and Tildesley 1987; Frenkel and Smit 2001) between the thermal conductivity and the time integral of the heat current autocorrelation function. The bulk thermal conductivities predicted with EMD and NEMD are in good agreement with experimental results (Volz and Chen 1999; Lukes, Li et al. 2000; Volz and Chen 2000; Schelling, Phillpot et al. 2002) and are within the statistical error of each other (Schelling, Phillpot et al. 2002). Previously, MD methods have been successfully used to predict the bulk thermal conductivity of crystalline materials, such as pure argon (Lukes, Li et al. 2000), diamond (Che, Cagin et al. 2000) and silicon (Volz and Chen 1999; Volz and Chen 2000), SiGe (Volz, Saulnier et al. 2000) and GaAs (Daly and Maris 2002) superlattices, silicon nanowires (Volz and Chen 1999), silica based crystal (McGaughey and Kaviany 2002) and amorphous materials, silicon (Lee, Biswas et al. 1991) and germanium (Ding and Andersen 1986). The out-of-plane thin-film thermal conductivities have been predicted using non-equilibrium MD (Lukes, Li et al. 2000; Feng, Li et al. 2001; Choi and Maruyama 2003; Feng, Li et al. 2003; Chantrenne and Barrat 2004). These studies focus on solid argon (Lukes, Li et al. 2000; Feng, Li et al. 2001; Choi and Maruyama 2003; Chantrenne and Barrat 2004) and on silicon at 500 K (Feng, Li et al. 2003).

Another approach to simulate phonon transport properties is Monte Carlo simulation. In the MC simulation, self-consistent calculation must be guaranteed, in which an assumed distribution function of phonons $f(k)$ is used to evaluate scattering

probabilities and the same $f(k)$ must be obtained as the solution. Since the electron-electron interactions do not significantly affect electron transport properties in semiconductors, they are often neglected in the traditional MC simulation. Several efforts carried out to account for electron-electron interactions have met with only partial success and these interactions remain a difficult problem to treat. The MC method cannot be directly implemented to solve the BTE for phonon transport since phonon-phonon interactions must be included in the simulation of phonon transport. Phonon-phonon scattering processes and phonon relaxation times or lifetimes are the basis of phonon transport. Only at extremely low temperature, where ballistic transport arises, is the phonon-phonon interaction unimportant. In 1988, Klitsner *et al.* applied the MC method to study ballistic phonon transport and found good agreement with theoretical analysis (Klitsner *et al.* 1988). Later Peterson simulated phonon transport using a MC method based on the Debye model, in which all of the phonons were assumed to have the same propagating speed, and no interactions between phonons were accounted for by assuming an average lifetime (Peterson 1994). With these assumptions, heat transfer in a one dimensional cell array was simulated and the time evolution of temperature profile was predicted. In 2002, Mazumdar and Majumdar reported MC simulation results for phonon transport in thin Si films (Mazumder et al. 2002). In their work, different phonon polarizations and phonon dispersions were taken into account by considering the dependence of phonon lifetime on frequency, polarization, and temperature. Their simulation results agreed well with the experimental data for temperatures lower than room temperature. Chen et al. used MC simulation method to calculate the thermal conductivity of silicon nanowires of various diameters for a wide temperature range

(Chen et al. 2005). Pop et al. have used Monte Carlo simulation method to estimate the heat generation in electronic nanostructures (Pop et al. 2002).

Boltzmann Transport Equations (BTE) can be solved analytically or numerically. To obtain a solution for BTE one needs to invoke many approximations. An equilibrium phonon distribution and scattering rate need to be estimated. This can make the solution deviate from actual experimental data. On the other hand, Monte Carlo (MC) simulation follows the trajectories of phonons in a solid. It uses the scattering mean free time which has been developed based on bulk material properties. However it does not need any approximation or simplification like BTE does. Ultimately however, both of them solves phonon transport and gives their distribution. However, the main shortcomings of MC simulation is i) the bulk material phonon dispersion is used and ii) it does not treat the surface realistically, i.e. it does not consider surface reconstruction. When the surface becomes important and the lengthscale becomes comparable to the wavelength of phonon, in which case the bulk phonon dispersion may not hold, then Molecular Dynamics (MD) simulation can be very helpful. MD simulation builds the model atom by atom, and doesn't rely on the bulk phonon dispersion. Also the real surface reconstruction can be seen in MD simulation. One drawback of MD simulation is that due to huge number of atoms, the lengthscale that can be simulated is bound by the computational power. Whereas in MC simulation, a large number of phonons is represented as a single phonon, thus reducing the computational burden, and enabling us to simulate larger system.

1.2 OBJECTIVE

The objectives of this dissertation are to employ nanoscale thermal transport simulation methods to better understand thermal transport at nanometer scale point and line constrictions and in nanowires of sawtooth surface roughness.

1.3 ORGANIZATION OF THIS DISSERTATION

Chapter 2 of the dissertation describes molecular dynamics simulation of thermal transport at a nano point contact between two silicon substrates. Detailed description of the computation method results and discussions are addressed in the chapter. Chapter 3 discusses the molecular dynamics simulation results of thermal transport at a nano line contact between two silicon substrates. Chapter 4 describes Monte Carlo (MC) simulation of phonon transport in a 22 nm diameter silicon nanowire with sawtooth surface roughness. Chapter 5 summarizes the major findings of this dissertation.

Chapter 2 Molecular Dynamics simulation of thermal transport at a nanometer scale constriction in silicon

2.1 INTRODUCTION

Thermal transport across nanometer scale point and line constrictions and interfaces plays an important role in a number of technologies. Nanoscale point constrictions can be found in the tip-sample contacts of scanning probe microscopes, thermally assisted magnetic recording, and carbon nanotube thermal interface materials. Recently, Lyeo *et al.* reported an ultrahigh vacuum (UHV) scanning thermoelectric microscopy method (SThEM) for probing the local Seebeck coefficient (*S*) of nanostructured thermoelectric materials (Lyeo et al. 2004). In this method, an atomically sharp metal tip makes a nanometer size contact on a heated semiconductor sample, creating a large temperature gradient possibly of order 10^{10} K/m at the contact. The local temperature gradient causes carrier diffusion and results in a thermoelectric voltage that is proportional to the local Seebeck coefficient of the non-uniform temperature zone.

The size of the resulting non-uniform temperature zone in the semiconductor determines the spatial resolution of the measurement, which appears to be about two times of the average nearest-neighbor inter-dopant distance of 4-10 nm in the doped GaAs samples. Because this length scale is comparable to the mean free paths of phonons and electrons, these energy carriers can have non-equilibrium energy distributions at the contact. Consequently, their temperature distributions cannot be obtained with the use of the heat diffusion equation.

The same issue is also present for a recently reported method for scaling down the bit size and increasing the data density in magnetic data storage. In this thermally assisted recording (TAR) method, (Harman et al. 2004) a heated tip is brought in close proximity to a magnetic film with a high magnetic anisotropic energy density. The hot tip raises the local film temperature so that data can be written locally to a bit as small as 50 nm when a magnetic field is applied. Adequate models are lacking for calculating the spatial extent of the heated zone that limits the bit size.

Moreover, the super high thermal conductivity of carbon nanotubes has inspired several experimental efforts where CNTs are employed as thermal interface materials for electronic packaging (Chuang et al. 2004; Xu et al. 2004). One intriguing problem in these efforts is the thermal resistance at the nanometer point contacts between a CNT and a planar surface. One measurement result has suggested that this resistance is rather high, but the mechanism is not well understood (Hu et al. 2005).

Meanwhile, Bi-based and III-V nanowire materials have been investigated for improving the energy efficiency of thermoelectric refrigerators and power generators (Lin et al. 2000; Mingo 2004). In nanowire thermoelectric devices, phonon and electron transport across nanoscale point contacts between the nanowires and the metal electrode can play a very important role on the device performance.

There have been extensive theoretical studies of the thermal resistance of a point contact between two solid materials (Madhusudana 1996; Cooper et al. 1968). Two expressions of thermal resistance at a point constriction can be obtained, one for the macroscopic diffusive resistance at the Maxwell's limit where the radius of the constriction (a) is much larger than the phonon mean free path (l) in the bulk material, *i.e.*

the Knudsen number $K \equiv l/a << 1$, and another for the ballistic resistance at the Knudsen limit of $K >> 1$. Wexler unified these two limiting cases and introduced a single equation for the thermal resistance of an orifice by adding up the diffusive resistance (R_d) and ballistic resistance (R_b) (Wexler 1966):

$$R = \gamma(K) R_d + R_b, \tag{2.1}$$

where $\gamma(K)$ is a slowly varying function with $\gamma(0) = 1$ and $\gamma(\infty) = 0.694$. The diffusive resistance is calculated to be (Madhusudana 1996):

$$R_d = 1/2ka, \tag{2.2}$$

where k is the thermal conductivity.

The ballistic thermal resistance can be calculated as follows (Sharvin 1965; Weber et al. 1989; Little 1959; Nikolic et al. 1999). By integrating the ballistic phonon flux from different directions through a constriction or orifice with radius a much smaller than l, one can obtain the net heat current transferred through the orifice as:

$$q = \frac{\pi a^2}{4} \Delta T \int_{\omega=0}^{\infty} v_g \frac{\partial < n_0 >}{\partial T} D(\omega) \hbar \omega d\omega \tag{2.3}$$

where ΔT is the temperature difference between the phonons immediately at the two sides of the constriction, v_g is the phonon group velocity, $<n_0>$ is the occupation of phonons given by the Bose-Einstein distribution corresponding to the local equilibrium temperature T, $D(\omega)$ is the phonon density of states at frequency ω, and $\hbar$ is the Planck's constant. The ballistic thermal resistance is obtained as

$$R_b \equiv \frac{\Delta T}{q} = \left(\frac{\pi a^2}{4} \int_{\omega=0}^{\infty} v_g \frac{\partial < n_0 >}{\partial T} D(\omega) \hbar \omega d\omega \right)^{-1} \tag{2.4}$$

If the phonon group velocity is assumed to be independent of frequency, Eq. (2.4) is reduced to

$$R_b = 4/(Cv_g \pi a^2) \tag{2.5}$$

If the phonon mean free path is also independent of frequency, Eq. (2.5) can be further expressed according to the thermal conductivity expression $k = Cv_g\, l/3$ to be

$$R_b = 4l/(3\pi k a^2) = 4K/(3\pi k a) \tag{2.6}$$

However, phonon group velocity and mean free path is not independent of frequency, thus this form of solution will give erroneous results. It is assumed in this analytical model that the deviation from the equilibrium distribution is small. This assumption is inappropriate for SThEM and other nanoscale point contacts, where large non-equilibrium prevails locally at the contact point. Moreover, Eq. (2.4) assumes complete phonon transmission at the constriction. This is a limiting case because atomic reconstruction can occur in a realistic constriction, potentially reducing the phonon transmission coefficient. When the constriction size is smaller than the dominant phonon wavelength (λ_0), Rayleigh scattering of phonons can also reduce the transmission coefficient according to Prasher et al (Prasher 2006). Furthermore, the temperature distribution at the constriction is not given by this model.

To better understand thermal transport at nanoscale constrictions, here we report a theoretical study of highly non-equilibrium thermal transport at a nanoscale constriction in silicon using Non Equilibrium (NE) Molecular Dynamics (MD) simulation. The simulation method and results are discussed in the following sections. We have not used Monte Carlo simulation to solve this problem for the following reasons i) MC uses the

bulk material phonon dispersion which can deviate substantially when the lengthscale is comparable to the phonon wavelength ii) MC does not treat the surface realistically, i.e. it does not consider surface reconstruction.

2.1 SIMULATION METHOD

The MD technique is a deterministic non-quantum computational method, used to predict the trajectory of an ensemble of atoms by solving Newton's second law of motion for each atom:

$$m_i \frac{d^2 \vec{x}_i}{dt^2} = \vec{F}_i = -\vec{\nabla}_i U \tag{2.7}$$

where m_i and x_i are the mass and location of i^{th} atom. The total force F_i on atom i is due to the interaction with all the atoms in the ensemble, and is calculated by taking the gradient of the potential energy U.

We have used a NEMD method to simulate thermal transport across a circular constriction formed between two Si (100) substrates, as shown in Fig. 2.1. The simulation box is a cube, for which the length in each of the three dimensions is 200 nm. There are about 400 million atoms in the cube. Atoms were arranged in diamond lattice structure and the simulation box coincides with the [100], [010] and [001] directions. The simulation box has been divided into two parts. The top half and the bottom half represent two Si substrates with their (100) surfaces facing each other. At the interface of the two Si substrates, there is a phonon blocking partition with a small circular constriction or orifice at the center that allows phonon transport between the two parts. It is assumed that except at the central constriction the surface atoms at one side of the phonon blocking partition do not have force interaction with the atoms at the other

surface. The two surfaces at the two sides of the partition are thus equivalent to two free surfaces facing each other without any energy transfer between them except at the constriction. In the simulation, the outer walls of the top part are maintained at temperature T_1, and the outer walls of the lower part are maintained at a different temperature T_2.

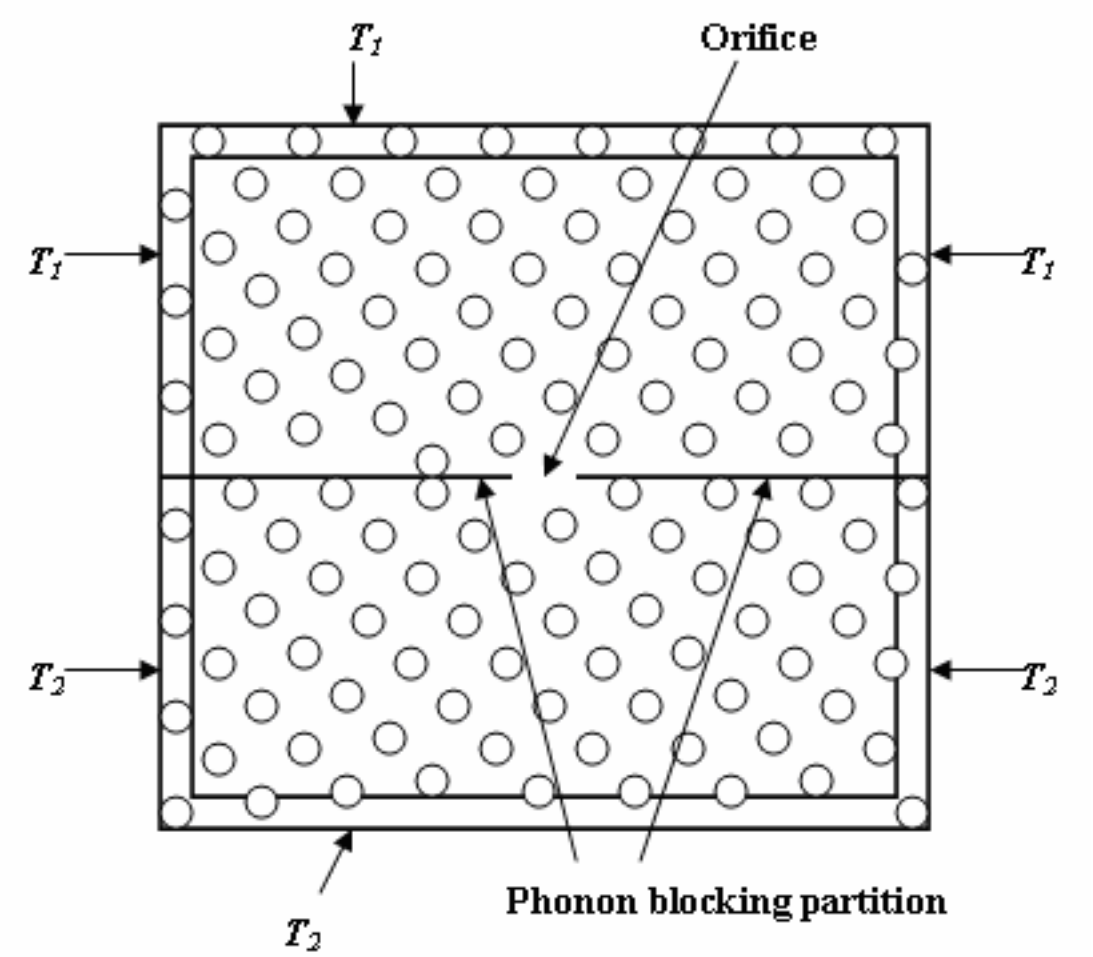

FIG. 2.1: Schematic diagram of the simulation box. The initial temperature is 300 K. T_1 = 340 K and T_2 = 300 K.

Because the electron contribution to heat conduction in silicon is small, an atomistic model such as the MD method that ignores electron transport is appropriate for

the current problem. Further, a MD simulation can deal with highly non-equilibrium situations and can reveal atomic reconstruction at the surfaces. For this reason, this approach is appropriate for the problem of nanoscale constrictions and interfaces.

Because one of our objectives is to find the temperature profile at the nano-constriction, we have used the direct method that relies on imposing a temperature gradient across the simulation cell (Maiti et al. 1997; Schelling et al. 2002; Jund et al. 1999), instead of the Green-Kubo approach (Che et al. 2000; Volz et al. 1999), which is an equilibrium MD method that uses current fluctuations to compute the thermal conductivity via the fluctuation-dissipation theorem.

Among the interatomic potentials available for silicon, the Stillinger-Weber (SW) potential (Stillinger and Weber 1985) accurately predicts temperature related properties, such as the melting point (Stillinger and Weber 1985; Broughton and Li 1987) and the thermal expansion of silicon (Cook and Clancy 1993), as well as the elastic properties (Karimi, Yates et al. 1998) and the yield strength (Kallman, Hoover et al. 1993).

The SW potential utilizes two and three body interaction terms to stabilize the diamond lattice that consists of atoms held in place by strong and directional bonds. The reduced pair potentials are described as follows:

$$f_2(r) = \begin{cases} A(Br^{-p} - r^{-q})\exp[(r-a)^{-1}], & r < a \\ 0, & r \geq a \end{cases} \tag{2.8}$$

where r is the distance between atoms, a is the cut off radius, and A, B, p, q are fitting parameters. This generic form automatically cuts off at $r = a$ without discontinuities in any r derivatives. The three body interaction term is written as

$$f_3(r_i, r_j, r_k) = f_{3a}(r_{ij}, r_{ik}, \theta_{jik}) + f_{3b}(r_{ji}, r_{jk}, \theta_{ijk}) + f_{3c}(r_{ki}, r_{kj}, \theta_{ikj}) \tag{2.9}$$

where

$$f_{3a}(r_{ij}, r_{ik}, \theta_{jik}) = \begin{cases} \lambda \exp[\gamma(r_{ij} - a)^{-1} + \gamma(r_{ik} - a)^{-1}](\cos\theta_{jik} + 1/3)^2, r_{ij} \text{ and } r_{ik} < a \\ 0, r_{ij} \text{ and } r_{ik} > a \end{cases} \quad (2.10)$$

The term f_{3a} vanishes for θ_{ijk} = $\cos^{-1}(-1/3)$, favoring ideal tetrahedral bond. In these formulae, r is the distance between two atoms and θ_{jik} is the angle at the vertex at particle i of the triplet. The parameter values are A = 7.049, B = 0.602, p = 4, q = 0, λ = 21.0, and γ = 1.2. At the phonon blocking partition, the potential between the two (100) Si substrates is switched off and the two substrates interact with each other through SW potential only at the central constriction. Except at the constriction, the two surfaces at the two sides of the partition are treated as two free surfaces following the method by Volz and Chen (Volz and Chen 1999).The integration method used for our Molecular Dynamics simulation is the Predictor-Corrector method (Rapaport 2004).

We have investigated the case of uniform boron doping in the entire simulation box because boron is a common doping element in Si. Particles designated as dopants differ from silicon atoms in both the atomic mass and their interactions with their neighbors. In order to introduce some mismatch, the values of potential parameters A and B are changed to values that lead to an increase in the interatomic spacing between silicon and boron. Hence, the location of potential minima will be shifted to a slightly larger atomic spacing. Only substitutional doping atoms were considered in this work. Although interatomic spacing between a substitutional boron atom and a neighboring silicon atom is larger than that between two neighboring silicon atoms, the diamond lattice structure remains the same. Consequently, the three-body potential that stabilizes

the diamond lattice structure is the same for silicon and impurity. Following Kelly and Ungar (Kelly and Ungar 1990), we have chosen values for A and B as A = 8.535, B = 0.80 for the impurity atoms. The location of the potential minimum for these parameters is about 2.45 Å, as compared to 2.35 Å for silicon-silicon interaction. The mass of the impurity atom is taken to be the atomic mass of boron.

To implement the isothermal wall condition for the outer walls of the computation box shown in Fig. 2.1, we have employed the method of Maiti *et al*. 1997. For the constant-temperature boundary condition, the heat current is calculated as following (Bhattacharya et al. 2004; Lee et al. 1991):

$$\boldsymbol{q}(t) = \left(\sum_{i=1}^{N} \boldsymbol{v}_i \tilde{E}_i + \sum_{i=1}^{N} \sum_{j=1}^{N} (\boldsymbol{F}_{ij} \cdot \boldsymbol{v}_i) \boldsymbol{r}_{ij} \right) \Big/ V \tag{2.11}$$

where $\boldsymbol{q}(t)$ is the instantaneous heat current, $\boldsymbol{F}_{ij}$ is the force and $\boldsymbol{r}_{ij}$ is the distance between the i^{th} and j^{th} particle, V is the volume. $\tilde{E}_i$ is the total excess energy defined by:

$$\tilde{E}_i = \sum_j f_2(r_{ij}) + \sum_j \sum_k f_3(r_{ij}, r_{jk}, r_{ki}, \theta_{ijk}, \theta_{jki}, \theta_{kij}) + \frac{1}{2} m_i v_i^2 - h_i \tag{2.12}$$

where h_i is the enthalpy of the i^{th} atom, $f_2(r_{ij})$ is the pair potential energy and $f_3(r_{ij}, r_{jk}, r_{ki}, \theta_{ijk}, \theta_{jki}, \theta_{kij})$ is the three body potential.

When a temperature gradient is applied in the NEMD simulation, the center of mass of the entire system tends to drift (Jund and Jullien 1999). The drift can result in an inaccurate measurement of the actual local temperature. We have used the velocity-rescaling algorithm of Jund and Jullien that eliminates the drift (Jund and Jullien 1999)..According to this algorithm the modified velocity at each iteration is given by

$$v_i' = v_G + \alpha(v_i - v_G) \tag{2.13}$$

where v_G is the velocity of the center of mass of the ensemble of atoms in the domain selected for velocity rescaling and

$$\alpha = \sqrt{1 \pm \frac{\Delta\varepsilon}{E_c^R}} \tag{2.14}$$

The + (or –) sign in Eq. (2.14) applies to the case when the atoms are in the domain where heat is added (or removed). For the constant temperature boundary condition, $\Delta\varepsilon$ is the difference in the total kinetic energy of the atoms in the domain before and after the constant temperature boundary condition is maintained. The relative kinetic energy E_c^R is given by

$$E_c^R = \frac{1}{2}\sum_i m_i v_i^2 - \frac{1}{2}\sum_i m_i v_G^2 \tag{2.15}$$

For this direct MD method, it is important to establish a steady-state heat current flow. This amounts to obtaining a stationary temperature profile as a function of time, thus insuring that only a steady-state current is allowed. It was found by Maiti *et al*. 1999, that long simulations of about 1×10^{-9} s were necessary to achieve a smooth temperature profile for a Si grain boundary system.

In this work, we found that a steady state heat current was obtained for a total simulation time of 1.1×10^{-9} s, or 2×10^6 MD steps with each MD time step being 0.55×10^{-15} s, as discussed in the following. We used a grid system to divide the simulation box, with each grid volume consisting of about 49 atoms. The average temperature of the

atoms in each grid was calculated. The averaging was performed over a large number of MD steps according to

$$\frac{1}{M}\sum_{j=0}^{M-1}\sum_{i=1}^{n} m v_i^2 = \frac{3}{2}\frac{n}{N_{tot}}\int \langle n_0 \rangle \hbar\omega D(\omega) d\omega \qquad (2.16)$$

where M is the number of steps on which the averaging is performed, m is the mass of the silicon atom, v_i is the velocity of the i^{th} atom, n is the number of atoms in the cell, and N_{tot} is the total number of atoms in the simulation. Phonon dispersion for bulk silicon based on Stillinger-Weber potential was used in the right hand side of Eq. (2.16), and the temperature contained in the $\langle n_0 \rangle$ term is solved numerically from Eq. (2.16) (Li et al. 1988). Here, although the MD simulation treats the vibrating atoms as classical particles, the total kinetic energy of the system is mapped onto the appropriate phonon distribution function $\langle n_0 \rangle$ according to Eq. (2.16) in order to correctly define the temperature. A common practice of defining the temperature using the formula $\frac{1}{2}\sum_i m v_i^2 = \frac{3}{2} n k_B T$ would be erroneous for the current problem as the temperature of interest is much lower than the Debye temperature of silicon.

The total number of steps in the simulation is N, and thus M must be smaller than N-1. For small M, the fluctuations in the obtained time-averaged temperature are entirely statistical and not due to transient effects related to the heat current sources. As M increases, fluctuations due to transient effects may be observed. Figure 2.2(a) shows the time-averaged temperature of the grid space at the center of the constriction for a 200 nm size box and a doping concentration of 3×10^{20} cm^{-3}. Each temperature point in the curve was the averaged value for 5000 MD steps. The averaging eliminates large temperature

fluctuation. As shown in Fig. 2.2(a), the system achieves steady state after about 1×10^6 MD step. Hence, 2×10^6 MD step is sufficiently long for obtaining the time-averaged temperature profile and steady-state heat current. Because of the large number (400 million) of atoms in the simulation box, it took about 30 days for each simulation that was run in dedicated Linux computer clusters to achieve steady state. Two of these workstations were equipped with four dual core Xeon processors with 8 GB of memory. Other workstations were equipped with Xeon processor and 2 GB memory.

At both sides of the partition, the heat current across the outer walls of rectangular boxes of different vertical depths measured from the constriction was calculated. The width of the rectangular boxes is twice of the depth. The heat current was calculated for each individual grid cell on the outer walls of the rectangular box and added up to obtain the total heat current across the outer walls. The heat current calculation for each cell was based on Eq. (2.11) and was averaged over the last 8×10^5 steps. As shown in Fig. 2.2(b), the difference between the total heat current across boxes of different depths is within 10%. The average value of all the heat current data calculated for different depths was used for thermal resistance calculation.

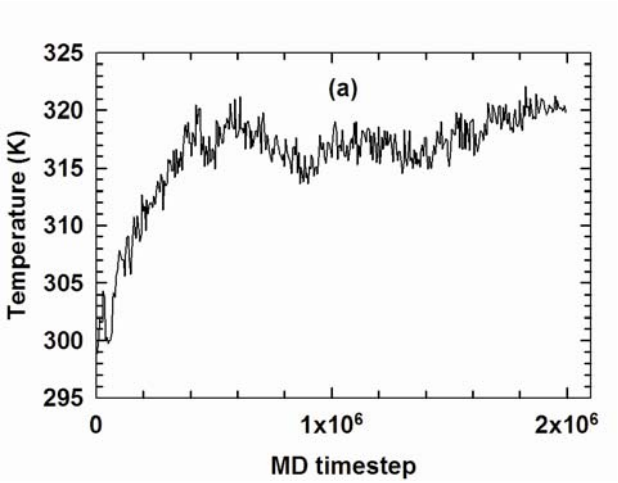

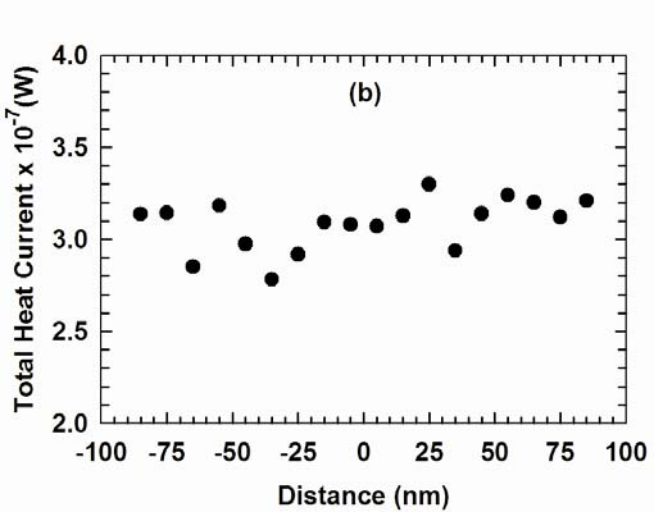

FIG. 2.2: (a) Time averaged temperature of the grid space at the center of the constriction for a constriction radius of 2 nm and doping concentration of 3×10^{20} cm^{-3}. (b) Time averaged total heat current across the boundaries of rectangular boxes at different vertical distances or depths measured from the constriction. The width of the box is twice of the depth.

Figures 2.3(a) and 2.3(b) shows the two dimensional (2D) projection of the atoms inside a 2 nm thick, 12 nm high, 12 nm wide rectangular box centered at the constriction

at the beginning and at the completion of the simulation, respectively. The atoms are positioned in a diamond lattice structure in Fig. 2.3(a); whereas in Fig. 2.3(b) the surface atoms become disordered, indicating that surface reconstruction occurs as simulation proceeds.

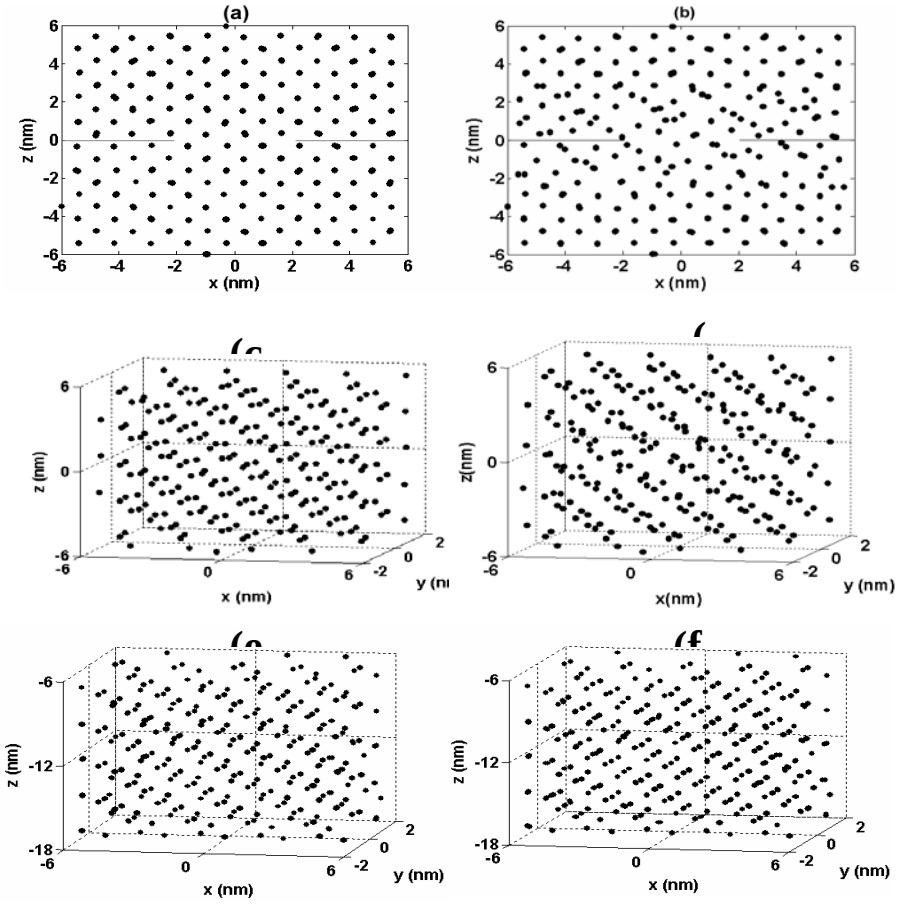

FIG. 2.3: (a)Two-dimensional projection of atoms in a 4 nm deep, 12 nm high, and 12 nm wide box centered at the constriction at the beginning, and (b) at the completion of the simulation; (c) Three-dimensional projection of atoms in a 4 nm deep, 12 nm high, and 12 nm wide box centered at the constriction at the beginning, and (d) at the completion of the simulation; (e) Three-dimensional projection of atoms in a 4 nm deep, 12 nm high, and 12 nm wide box away from the free surface at the beginning, and (f) at the completion of the simulation;

Fig. 2.3(c) and 2.3(d) shows the same figures in a three-dimensional projection. Fig 2.3(e) and 2.3(f) shows three dimensional projection of atoms away from the surface. The reconstruction occurs mainly within 2 nm distance from the two free surfaces at the partition. Because of the reconstruction, the two free surfaces become rough. The roughness can lead to diffuse phonon-surface scattering.

As a bench-mark experiment to check the correctness of the MD code, we have modified the code according to Schelling *et al.*'s procedure to calculate the thermal conductivity of solid Si (Schelling et al. 2002). The calculated thermal conductivity at T = 155 K, 255 K and 300 K are 322 W/m-K, 163 W/m-K and 119 W/m-K, respectively, in agreement with Schelling *et al.*'s simulation results and the measurement results in the literature (Schelling et al. 2002; Glassbrenner and Slack 1964).

2.2 SIMULATION RESULTS AND DISCUSSIONS

The temperature profile on the vertical plane passing through the center of the constriction is plotted in Fig. 2.4 where the doping concentration is N_d = 3 x 10^{20} atoms/cm^3. To compute the time-averaged spatial temperature distribution, we have used the results for the final 8 x 10^5 MD steps and have left out the data for the initial 1.2 x 10^6 MD steps. This procedure ensures that we have allowed sufficient time so that the system can reach steady state and the result does not consist of any transient effects.

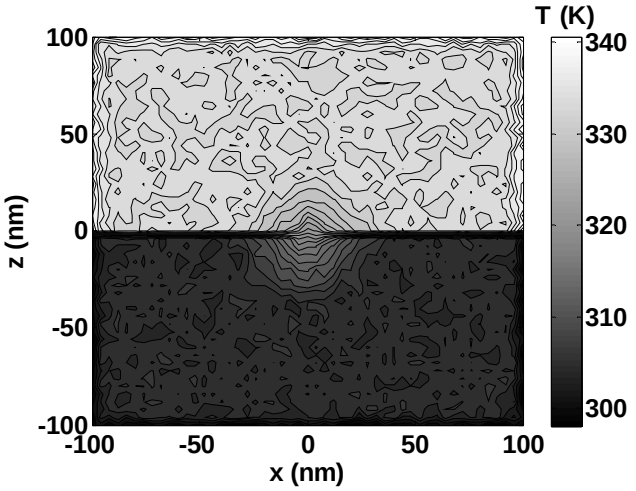

FIG. 2.4. Temperature distribution on the vertical section passing through the center of the constriction with a constriction radius of 2 nm, a boron doping concentration of 3 x 10^{20}/cm^3.

Figure 2.5 shows the temperature profile along the vertical axis passing the center point of the constriction. There is a temperature drop of about 28 K at the constriction and a drop of about 6 K each at the upper and lower walls of the simulation box.

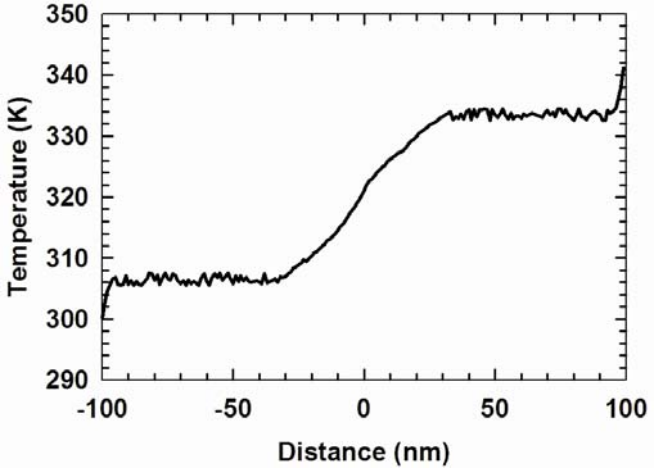

FIG. 2.5: Temperature profile along the vertical axis passing the center of the constriction as a function of the distance from the constriction. The constriction radius is 2 nm. The doping concentration is N_d = 3 x 10^{20} cm^{-3}.

The temperature drops at the boundary is believed to be an artifact caused by enforced phonon scattering at the heat source and sink (Maiti et al. 1997; Schelling et al. 2002). There is a flat temperature region between the outer boundaries and the constriction, indicating that the artifacts due to the enforced phonon-boundary scattering at the outer boundaries diminish in this flat temperature region as well as near the constriction. We have used the temperature drop across the constriction and between the two flat temperature regions for calculating the thermal resistance, thus eliminating the influence of the heat source or sink effect at the outer boundaries. Moreover, reducing the simulation box from 200 nm to 120 nm in each dimension would not change the temperature profile and temperature drop across the constriction. This was verified by simulation with a box size of 120 nm in each dimension. Hence, the 200 nm size simulation box is large enough to impose the isothermal boundary condition at the outer walls.

2.2.1 Effect of the Constriction Radius

We have examined the effect of the constriction radius (a) on the temperature distribution and thermal resistance of the constriction. We calculated the radius of the heated zone in the cold substrate as the distance (r_T) on the vertical axis from the center of the constriction for which $\Delta T(r_T) = T(r_T)-T_2 = 0.1\ (T_1-T_2)$. The resulting value of $\Delta T(r_T)$ is 4 K, which is small enough compared to T_1-T_2 and just slightly larger than the statistical precision of the simulation of about 2 K. Figure 2.6 shows the calculated r_T as a function of the constriction radius (a) in the range between 0.5 nm and 6 nm, for doping concentration of 3×10^{20} atoms/cm^3. The calculated r_T decreases rather slowly with decreasing a to approach about 20 times of the average nearest-neighbor inter-dopant

distance (d) that is estimated to be $d = (1/N_d)^{1/3} = 1.5$ nm, where N_d is the number density of impurity dopants. Because the smallest length scale within which thermal equilibrium can be obtained cannot be smaller than the phonon mean free path (l), r_T cannot be shorter than l when a is reduced below l. Hence, l at the constriction cannot be longer than $20d$ or 30 nm.

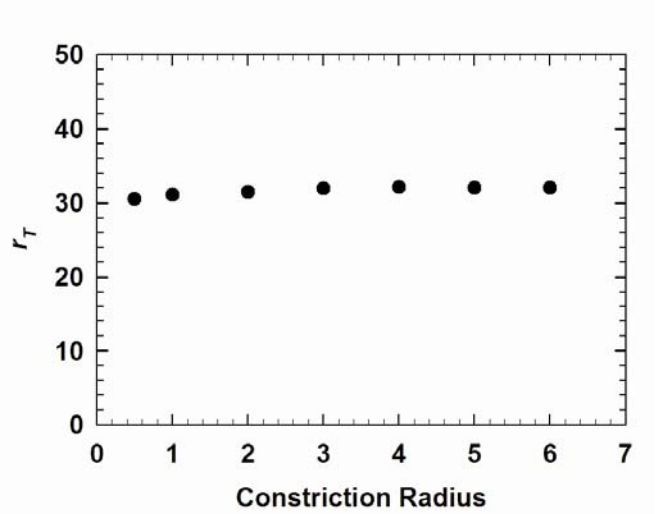

FIG. 2.6. r_T as a function of a for $N_d = 3 \times 10^{20}/\text{cm}^3$ corresponding to $d = 1.5$ nm.

We have calculated the bulk phonon mean free path (l) using a procedure where the phonon dispersion is taken into account (Chen 1998; Chen 1997). At room temperature, about one-third of the specific heat of Si is due to optical phonons. Since optical phonons have a very low group velocity, their contribution to the bulk thermal conductivity is negligible and one only needs to calculate the mean free path for the acoustic phonons based on the kinetic theory $k = Cvl/3$, where k, C, v, and l are the thermal conductivity, specific heat, group velocity, and mean free path, respectively, of

the acoustic phonons. In addition to excluding the optical phonons, we calculated the phonon group velocity from the phonon dispersion weighed over the relative contribution to the specific heat. Based on the calculation we obtained the heat capacity and group velocity of acoustic phonons at room temperature as C = 0.93 x 10^6 J/m^3-K, v = 1804 m/s. Using the experimental value of thermal conductivity for bulk silicon at the doping concentration of 3 x 10^{20}/cm, k = 50 W/m-K (Chen 1998; Chen 1997; Slack 1964), we calculated the bulk phonon mean free path to be l = 89 nm.

The obtained bulk l is about three times of r_T, which cannot be shorter than l at the constriction according to the above discussion. This discrepancy is attributed to a shorter l at the constriction than in the bulk. The shorter l is caused by frequent diffuse phonon scattering at the roughened free surface and phonon-impurity scattering at the vicinity of the constriction. Due to the interplay of these two scattering processes, phonons are scattered for multiple times by both the partition and impurity atoms before they escape the constriction. The short l in the vicinity of the constriction also explains that the diffuse outer walls do not introduce artifacts in the calculation results even when the bulk l is close to the vertical depth of the top or bottom part of the simulation box.

The thermal resistances of the constriction were calculated for a doping concentration of 3 x 10^{20}/cm^3 and different constriction radii, as shown in Fig. 2.7. In the MD simulation, the thermal resistance is calculated as $R = \Delta T/q$. Here, q is the total heat current calculated according to the above discussion and ΔT is the temperature drop at the constriction between the two flat temperature regions so that the temperature drops at the upper and lower walls of the simulation box are excluded from ΔT.

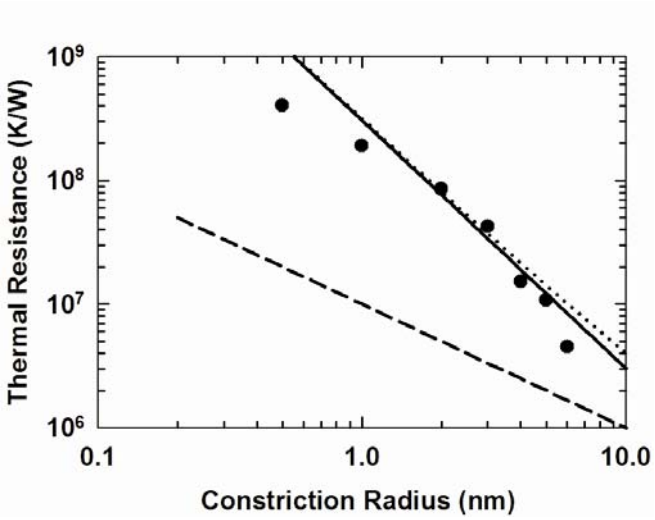

FIG. 2.7. The MD thermal resistance (filled circles) as a function of constriction radius (a) for N_d = 3 x 10^{20}/cm^3. Also plotted are R_b (solid black line) based on Eq. (2.4), R_d (dashed black line) from Eq. (2.2) with the use of the bulk k, and the total thermal resistance R (dotted line) calculated using Eqs. (2.1), (2.2), and (2.4).

Figure 2.7 also shows the total thermal resistance R calculated using Eqs. (2.1), (2.2), and (2.4). Here, $\gamma(K)$ is calculated following Wexler (Wexler 1966). Also plotted are the ballistic resistance R_b calculated from Eq. (2.4) and the diffusive resistance from Eq. (2.2). The Knudsen numbers corresponding to the constriction radius are larger than 9, well within the Knudsen limit, so that the obtained thermal resistance from Eq. (2.1) mainly comes from the ballistic resistance R_b from Eq. (2.4). The MD results were found to be close to R_b when the constriction radius is larger than 1 nm, indicating that surface reconstruction does not reduce the phonon transmission coefficient significantly. At a = 0.5 nm, however, the MD result is considerably lower than R_b. The discrepancy is attributed to the fact that bulk phonon dispersion and the SW potential are not longer

accurate at the constriction when a is reduced to be comparable to or smaller than the dominant phonon wavelength, which is about 1 nm in Si at 300 K.

2.2.2 Effect of the Doping Concentration

We have investigated the effect of the concentration of boron concentration N_d on r_T. N_d was varied from 10^{19} cm^{-3} to 10^{21} cm^{-3} with a fixed a = 2 nm. Figure 2.8 shows r_T together with the inter-dopant distance d as a function of N_d . At this constriction radius, r_T decreases with increasing doping concentration, and is about 20d. This feature manifests the interplay between diffuse phonon-surface scattering by the free surface and phonon-impurity scattering at the constriction. The observation of decreasing r_T with increasing doping concentration explains why the spatial resolution of SThEM was found to improve with increasing doping concentration in Lyeo *et al*'s experiment (Lyeo et al. 2004).

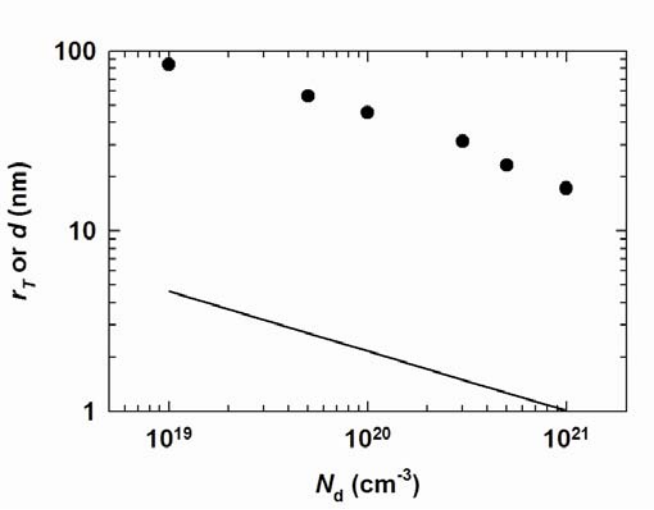

FIG. 2.8. r_T (open circles) and d (solid line) as a function of N_d for a = 2 nm.

The lack of alloy scattering in Si could have led to the larger l and r_T at the Si constriction considered here than in the III-V constriction in Lyeo et al.'s experiment. Nevertheless, the simulation result supports the experimental observation that the spatial resolution of SThEM and thus r_T can be smaller than the bulk phonon mean free path.

Figure 2.9 shows that the MD thermal resistance of the constriction increases slightly with N_d. Also shown in Fig. 2.9 are the total thermal resistance R calculated using Eqs. (1), (2), and (4) where the bulk k was used, and the ballistic resistance R_b from Eq. (2.4). The diffusive resistance R_d based on Eq. (2.2) is shown in the inset of the figure. For the calculation of R_d, k of bulk silicon at different doping concentrations was taken from literature (Slack 1964; Asheghi et al. 2002). It can be expected that doping has a much smaller effect on the phonon dispersion, specific heat, and group velocity that determine R_b than on l that affects k and R_d. Consequently, the increase in the thermal resistance with N_d should be mainly caused by the increase in R_d. In the calculation of R_b from Eq. (2.4) (as well as in the MD simulation), the phonon dispersion is assumed to be independent of the doping concentration, resulting in the constant R_b shown in Fig. 2.9 at different N_d. Note that the MD data increases more rapidly with N_d than the total resistance R from Eq. (2.1), although the amounts of increase are on the same order of magnitude. The use of the bulk k, which is larger than the effective k of the constriction, can underestimate R_d and yield the slower increase of the total resistance R with doping concentration.

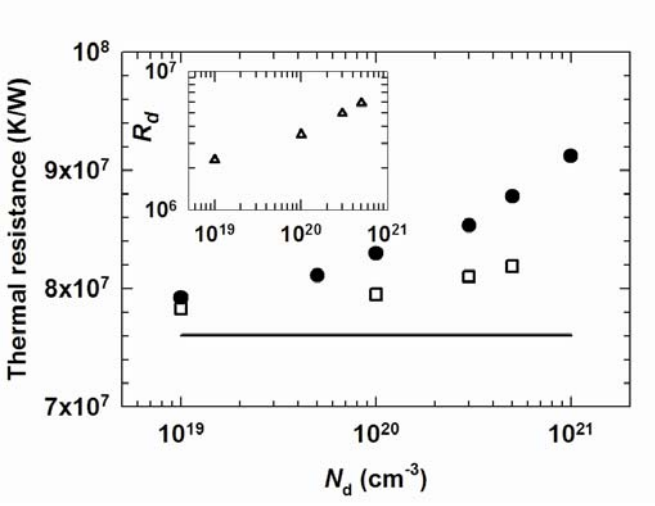

FIG. 2.9. MD thermal resistance (filled circles) of the constriction as a function of N_d for a = 2 nm. Also shown are R_b (line) from Eq. (2.4) and the total thermal resistance R (open squares) calculated using Eqs. (2.1), (2.2), and (2.4) with the use of the bulk k. The inset shows the obtained R_d from Eq. (2.2) with the use of bulk k.

2.3 CONCLUSIONS

The MD calculation reveals several phenomena that are not shown by the analytical model (Eq. 2.1). Most notably, the radius of the heated zone in the cold substrate was found to approach a limit of 15-17 times the average nearest-neighbor distance of impurity doping atoms when the constriction radius is reduced below the inter-dopant distance. Because this limit cannot be smaller than the phonon mean path at the constriction, the phonon mean free path at the vicinity of the constriction should be much shorter than the bulk value. The shorter mean free path is due to multiple phonon scattering events both by the two reconstructed free surfaces at the two sides of the partitions and by the impurity atoms before phonons escape from the constriction. The calculated thermal resistances of the constriction are close to the ballistic thermal resistance obtained from the analytical model and increases only slightly with increasing

doping concentration due to the increase in the diffusive resistance. These results can help to better understand thermal transport at the tip-sample contacts of various scanning probe microscopy methods and at the point contacts between a nanotube and a planar surface.

Chapter 3 Molecular Dynamics simulation of thermal transport at a nanometer scale line constriction in silicon

3.1 INTRODUCTION

Nano line interfaces are characteristic of nanoelectronic devices made of CNTs or semiconductor nanowires. For example, Si nanowire thin film transistor (TFT) devices have been fabricated on glass and on flexible, low-cost polymer substrates (Friedman et al., 2005). Although the nanowire TFT device show better performance than conventional TFT devices, the nano- line interface between the nanowire and the low-thermal conductivity substrate will likely creates a high thermal resistance and leads to a high operating temperature that negatively impacts device performance and reliability. It is difficult to calculate this nanowire interface resistance because the contact area is complex.

Nano line interfaces can also be found in the lower levels of metal interconnect line and via structures for future-generation ULSI devices. Thermal resistance between the nanoscale interconnect lines or vias and the dielectric medium is an important parameter for thermal management but has not been adequately characterized. The technological potential of this geometrical configuration is immense. Therefore it is very important to develop models for the thermal resistance of nano-sized curved surfaces such as spherical nanoparticles and cylindrical nanowires with a planar surface.

As shown in chapter 2, two types of thermal resistance exists for a constriction. One is the macroscopic diffusive resistance (R_d) at the Maxwell's limit where the half

width of the nanoline constriction (a) is much larger than the phonon mean free path (l) in the bulk material, *i.e.* the Knudsen number $K \equiv l/a << 1$, and the other being the ballistic resistance (R_b) at the Knudsen limit of $K >> 1$. The total constriction resistance can be calculated by summing the diffusive resistance (R_d) and ballistic resistance (R_b) (Prasher 2005):

$$R = R_d + R_b \tag{3.1}$$

The diffusive resistance is calculated to be:

$$R_d = \frac{2}{L\pi k_s} \ln\left(\frac{D}{\pi a}\right) \tag{3.2}$$

where L is the length of the line, D is the distance from the center of the line and k_s is the thermal conductivity of the substrate (Macgee et al. 1985; Bahadur et al. 2005)

The ballistic thermal resistance can be calculated similar to as shown in Chapter 2, Eq. (2.4) and can be written as:

$$R_b \equiv \frac{\Delta T}{q} = \left(\frac{A}{4} \int_{\omega=0}^{\infty} v_g \frac{\partial < n_0 >}{\partial T} D(\omega) \hbar \omega d\omega \right)^{-1} \tag{3.3}$$

For the case that the phonon group velocity is independent of frequency, Eq. (3.3) is reduced to

$$R_b = 4/\left(C v_g A\right) \tag{3.4}$$

If the phonon mean free path is also independent of frequency, Eq. (3.4) can be further expressed according to the thermal conductivity expression $k = Cv_g\, l/3$ to be

$$R_b = 4l/(3\pi kA) = 2K/(3kL) \tag{3.5}$$

To better understand thermal transport at a nanoline constriction, this chapter reports a theoretical study of highly non-equilibrium thermal transport at a nanoline constriction in silicon using Non Equilibrium (NE) Molecular Dynamics (MD) simulation. The simulation method and results are discussed in the following sections.

3.2 SIMULATION METHOD

The simulation setup is very similar to the setup described in Chapter 2. We have changed the size of the width of the simulation box from 200 nm to 20 nm, so that the simulation box size is 200 nm x 200 nm x 20 nm. Atoms were arranged in diamond lattice structure and the simulation box coincides with the [100], [010] and [001] directions. The simulation box has been divided into two parts. The top half and the bottom half represent two Si substrates with their (100) surfaces facing each other. At the interface of the two Si substrates, there is a phonon blocking partition with a nanoline constriction running through the center along the width that allows phonon transport between the two parts. This is shown in Fig. 3.1(a) and 3.1(b). Similar to the setup in Chapter 2, two surfaces at the two sides of the partition are equivalent to two free surfaces facing each other without any energy transfer between them except at the constriction. In the simulation, the top wall of the top part is maintained at temperature T_1, and the bottom wall of the lower part is maintained at a different temperature T_2. The side walls have periodic boundary condition to simulate infinitely long nanoline constriction.

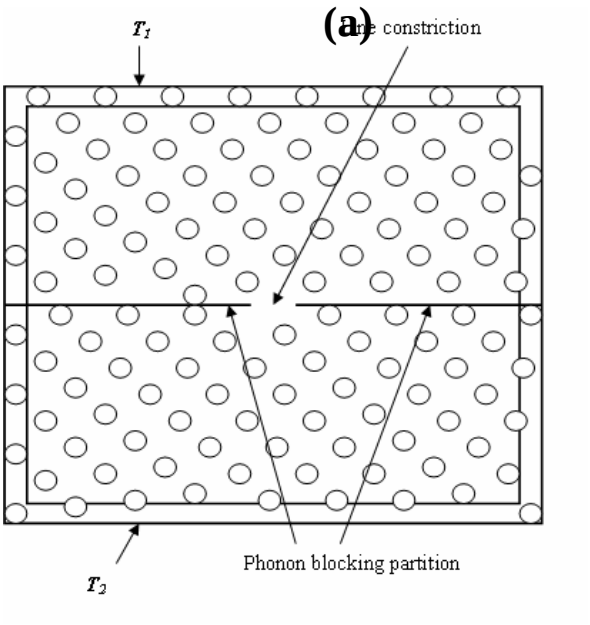

FIG. 3.1. (a) Two dimensional schematic diagram of the simulation box. The initial temperature is 300 K. T_1 = 340 K and T_2 = 300 K. (b) Three dimensional schematic diagram of the simulation box with nanoline constriction shown at the middle.

The Stillinger and Weber (SW) potential described in Chapter 2 has been used here. The integration method used for our Molecular Dynamics simulation is the Predictor-Corrector method. We have investigated the case of uniform boron doping in the entire simulation box. Details about the boron doping simulation method has been discussed in Chapter 2. We have used boron doping concentration of 3×10^{20} atoms/cm^3 for all the simulation run. The isothermal wall was implemented the same way as described in Chapter 2. The heat current is calculated the same way as given in Chapter 2 eq. (2.11). We have also applied the velocity-rescaling algorithm of Jund and Jullien to eliminate the drift as described in Chapter 2. In this work, we found that a steady state heat current was obtained for a total simulation time of 1.1×10^{-9} s, or 2×10^6 MD steps with each MD time step being 0.55×10^{-15} s. The gird system is the same that was used is Chapter 2. The temperature in each grid was calculated according to eq. (2.16).

3.3 SIMULATION RESULTS AND DISCUSSIONS

Figures 3.2(a) and 3.2(b) shows the two dimensional (2D) projection of the atoms inside a 2 nm thick, 12 nm high, 12 nm wide rectangular box centered at the constriction at the beginning and at the completion of the simulation, respectively. The atoms are positioned in a diamond lattice structure in Fig. 3.2(a); whereas in Fig. 3.2(b) the surface atoms become disordered, indicating that surface reconstruction occurs as simulation proceeds. This was also observed in Chapter 2 for the simulation of nanopoint contact.

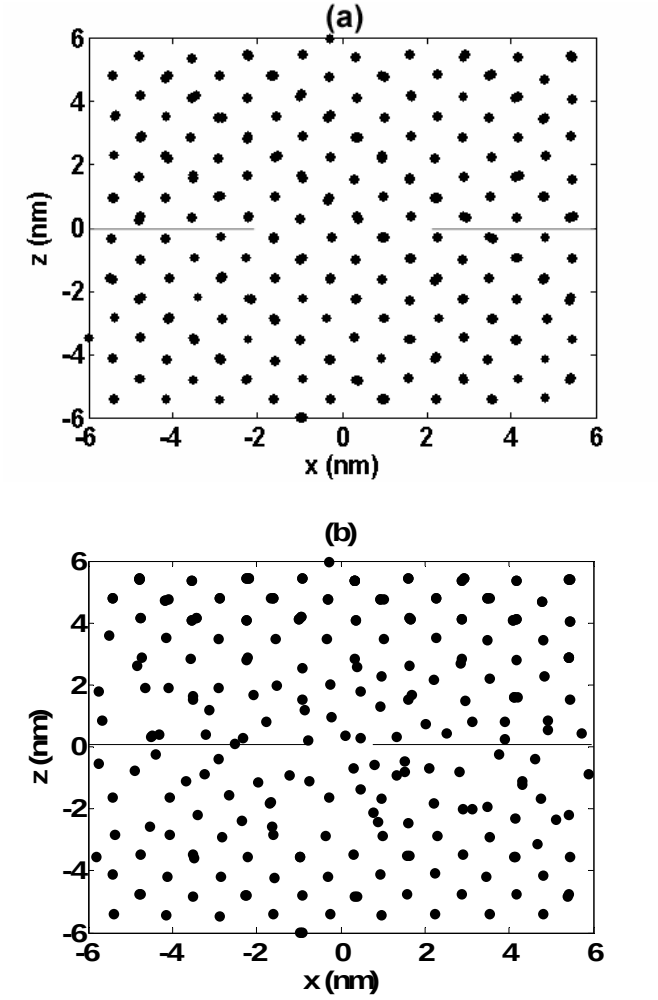

Fig. 3.2: (a)Two-dimensional projection of atoms in a 4 nm deep, 12 nm high, and 12 nm wide box centered at the nanoline constriction at the beginning, and (b) at the completion of the simulation

Figure 3.3 shows the temperature profile along the vertical axis passing the center point of the constriction. There is a temperature drop of about 28 K at the constriction and a drop of about 6 K each at the upper and lower walls of the simulation box. The temperature drop at the boundary is very similar to what we found for the nanopoint constriction simulation box in Chapter 2, and is believed to be an artifact caused by enforced phonon scattering at the heat source and sink (Maiti et al. 1997; Schelling et al.

2002). Compared to the nanopoint constriction, here also we find a flat temperature region between the outer boundaries and the constriction, indicating that the artifacts due to the enforced phonon-boundary scattering at the outer boundaries diminish in this flat temperature region as well as near the constriction. We have used the temperature drop across the constriction and between the two flat temperature regions for calculating the thermal resistance, thus eliminating the influence of the heat source or sink effect at the outer boundaries.

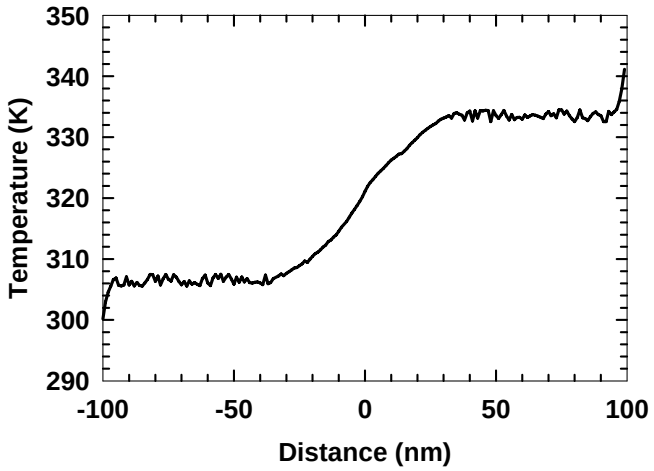

FIG. 3.3. Temperature profile along the vertical axis passing the center of the constriction as a function of the distance from the constriction. The nanoline constriction half width is 2 nm. The doping concentration is $N_d = 3 \times 10^{20}$ cm^{-3}.

We have examined the effect of the nanoline constriction half width (a) on the temperature distribution and thermal resistance of the constriction. We calculated the radius of the heated zone in the cold substrate as the function of distance (r_T) on the vertical axis from the center of the constriction for which $\Delta T(r_T) = T(r_T)-T_2 = 0.1\ (T_1-T_2)$.

The resulting value of $\Delta T(r_T)$ is 4 K, which is small enough compared to T_1-T_2 and just slightly larger than the statistical precision of the simulation of about 2 K. Figure 3.4 shows the calculated r_T as a function of the nanoline constriction half width (a) in the range between 0.5 nm and 6 nm, for doping concentration of 3×10^{20} atoms/cm^3. The calculated r_T decreases slowly with decreasing a, and is comparable to the value calculated in chapter 2. It approaches about 20 times of the average nearest-neighbor inter-dopant distance (d) that is estimated to be $d = (1/N_d)^{1/3} = 1.5$ nm, where N_d is the number density of impurity dopants. As stated in chapter 2, r_T cannot be shorter than the phonon mean free path (l) and since r_T is about 20d or 30 nm, hence l at the constriction cannot be longer than 20d or 30 nm. Because the smallest length scale within which thermal equilibrium can be obtained cannot be smaller than the phonon mean free path (l), r_T cannot be shorter than l when a is reduced below l. Hence, l at the constriction cannot be longer than 20d or 30 nm.

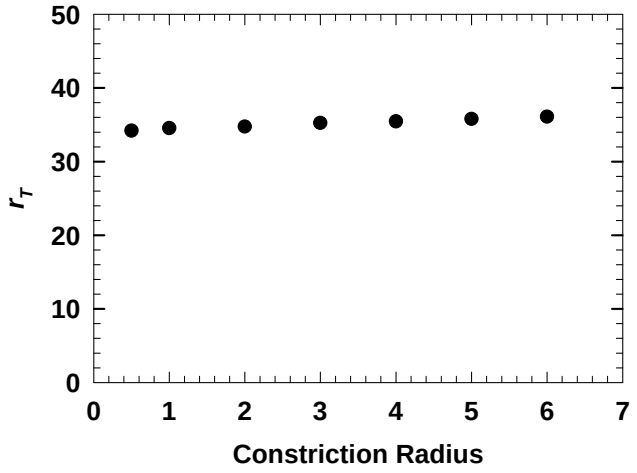

FIG. 3.4. r_T as a function of a for $N_d = 3 \times 10^{20}$/cm^3.

The bulk phonon mean free path has been calculated in Chapter 2 to be l = 89 nm. The obtained bulk l is about three times of r_T, which cannot be shorter than l at the constriction according to the above discussion. This discrepancy is attributed to a shorter l at the constriction than in the bulk which is explained in detail in Chapter 2..

The thermal resistances of the constriction were calculated for a doping concentration of 3 x 10^{20}/cm^3 and different nanoline constriction half width (a), as shown in Fig. 3.5. In the MD simulation, the thermal resistance is calculated as $R = \Delta T/q$. Here, q is the total heat current calculated according to Eq. (2.11) and ΔT is the temperature drop at the constriction between the two flat temperature regions. Figure 3.5 also shows the total thermal resistance R calculated using Eqs. (3.1), (3.2), and (3.3). The Knudsen numbers corresponding to the nanoline constriction half width a are larger than 9, well within the Knudsen limit, so that the obtained thermal resistance from Eq. (3.1) mainly comes from the ballistic resistance R_b from Eq. (3.3). The total resistance was 1-2 order magnitude higher than the diffusive resistance R_d, hence neglecting the ballistic resistance would give erroneous estimation of thermal resistance for Knudsen number K>1. The MD results were found to be close to R_b indicating that surface reconstruction does not reduce the phonon transmission coefficient significantly. The analytical solution is in close agreement with the MD simulation results.

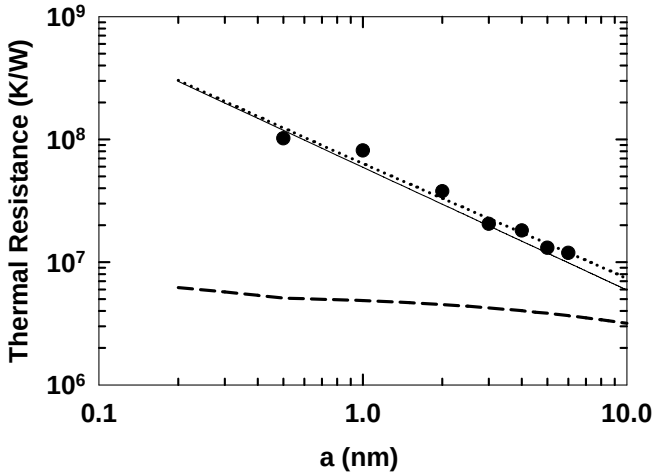

FIG. 3.5. The MD thermal resistance (filled circles) as a function of nanoline constriction half width (a) for N_d = 3 x 10^{20}/cm^3. Also plotted are R_b (solid black line) based on Eq. (3.3), R_d (dashed black line) from Eq. (3.2) with the use of the bulk k, and the total thermal resistance R (dotted line) calculated using Eqs. (3.1), (3.2), and (3.3).

3.4 CONCLUSIONS

MD simulation of the nanoline constrictions reveals similar results as those for nano point constrictions. The radius of the heated zone in the cold substrate was found to approach a limit of 20 times the average nearest-neighbor distance of impurity doping atoms when the constriction radius is reduced below the inter-dopant distance. The phonon mean free path at the constriction was found to be suppressed by diffuse phonon-boundary scattering and phonon-impurity scattering. MD thermal resistances of the constriction are close to the ballistic thermal resistance, suggesting that surface reconstruction does not reduce the phonon transmission coefficient at the constriction significantly.

Chapter 4 Monte Carlo Simulation of phonon transport in a silicon nanowire with sawtooth surface roughness

4.1 INTRODUCTION

Thermal transport in nanostructures such as nanowires and thin films are under intense investigation due their promise for various technologies such as high efficiency thermoelectrics (Chen and Shakouri 2002). They are also being investigated for understanding the physics of thermal transport at the nanoscale (Cahill et al. 2003). Two different size confinement effects can impact phonon transport in nanostructures. When the characteristic length of the nanostructure is reduced to be comparable to or below the bulk phonon mean free path, boundary scattering of phonons dominates, resulting in the suppression of the thermal conductivity (k) of the nanostructures below the corresponding bulk value. Phonon mean free path of bulk crystalline solids is typically in the range of a few to a few hundreds of nanometers at room temperature. When the characteristic length is reduced further to be comparable to or smaller than the dominant phonon wavelength (λ_0), which is about 1 nm in silicon at room temperature (Yang and Chen 2004), the phonon dispersion can differ from bulk dispersion, modifying the phonon group velocity and thermal conductivity. Owing to the very small λ_0 of phonons, unless the temperature is very low or the characteristic length is about 1 nm or smaller at room temperature, phonon dispersion in the nanostructures can still be described using the bulk dispersion and the main size effect on thermal conductivity is due to boundary scattering of phonons (Mingo 2003; Prasher 2006).

A great deal of experimental and theoretical studies of thermal transport in nanowires and thin films have been reported. Theoretical studies based on Boltzmann Transport Equation (BTE), Molecular Dynamics simulation and Monte Carlo (MC) simulations have been used to explain micro and nano scale heat transport phenomena in these nanostructures. The BTE is often the starting point for the theoretical analysis of phonon transport (Callaway 1959; Holland 1963; Armstrong 1985; Chen 2001). Based on the lifetime assumption and with some simplifications; it is possible to achieve a closed form analytical solution for the BTE. However, since many assumptions must be introduced to reach a closed form solution, the results usually deviate significantly from experimental observations. In 2002, Mazumdar and Majumdar reported MC simulation of phonon transport in thin Si films (Mazumder et al. 2002). In their work, different phonon polarizations and phonon dispersions were taken into account by considering the dependence of phonon lifetime on frequency, polarization, and temperature. Chen et al. used MC simulation method to calculate the thermal conductivity of silicon nanowires of various diameters for a wide temperature range (Chen et al. 2005). For the smallest diameter of 22 nm, their and other's calculation results differ significantly from the experimental data and cannot explain the unusually low thermal conductivity observed in the experiment (Li et al. 2003).

In all these studies, the surface was treated as flat. The effect of surface roughness was incorporated by introducing partially diffuse and partially specular scattering of phonons at the surface. Diffuse scattering refers to the case that phonons loose their memories and are reflected back at a random direction when they encounter the

boundary. Specular scattering is the case that phonons are reflected back following the Snell's law of reflection from the surface when they encounter the boundary,.

In the current literature boundary scattering of phonons is treated as either purely diffuse, purely specular or a combination of both (Ziman 1960). Purely diffuse scattering gives the lower bound of k and purely specular scattering yields no reduction in k assuming bulk phonon dispersion. The specularity parameter (p) is generally used as a fitting parameter for simulating the scattering from the interface (Mingo et al. 2003a; Mingo et al. 2003b; Dames et al. 2004). In the case of a nanowire of diameter d, the effective mean free path (l_B) due to boundary scattering is given by (Ziman 1960; Dames et al. 2004):

$$l_B = \frac{1+p}{1-p} d \tag{4.1}$$

For random surface roughness that obtains a Gaussian distribution, the specularity parameter p is usually evaluated using Ziman's formula as (Ziman 1960):

$$p = \exp(-16\pi^3 \delta^2 / \lambda^2) \tag{4.2}$$

where δ is the surface roughness and λ is the phonon wavelength. For perfectly smooth surface with δ several orders of magnitude smaller than λ_0, p from Eq. (4.2) approaches the upper bound of 1 corresponding to purely specular surface scattering. For even atomically smooth surface where the surface roughness is comparable to atomic corrugation of 0.2-0.3 nm, Ziman's formula yields a value of p approaching 0 for Si at room temperature with $\lambda_0 \approx 1$ nm. Corresponding to purely diffuse surface scattering, p = 0 yields the lowest thermal conductivity of a nanowire when the bulk dispersion is still

applicable. This limit is referred as the diffuse surface limit ($k_{diffuse}$) of nanowire thermal conductivity.

Most of the existing thermal conductivity measurement results of nanowires were found to be close to the diffuse surface limit (Li et al. 2003; Shi et al. 2004). For many of these semiconductor nanowires that are investigated for improving the energy efficiency of thermoelectric devices, the diffuse surface limit still yields a thermal conductivity much higher than state-of-the-art bulk or nanostructured thermoelectric materials.

It has been reported that gas molecules in a channel can be backscattered by a rough surface (Berman et al. 1972). Such backscattering can reduced the thermal conductivity below the diffuse surface limit. The question that we seek to answer in this letter is whether one can engineer the surface roughness on a nanowire to facilitate phonon backscattering so as to reduce the thermal conductivity below $k_{diffuse}$.

We note that nanowires of sawtooth surface roughness or zig-zag structures have been synthesized recently (Ross et al. 2005; Peng et al. 2007). Using Monte Carlo (MC) simulation, we show that phonon backscattering can indeed occur on such sawtooth nanowire surface, reducing the thermal conductivity below $k_{diffuse}$. Moreover, phonon backscattering at asymmetric sawtooth surfaces can further cause thermal rectification, resulting in direction dependant thermal conductance of a nanowire.

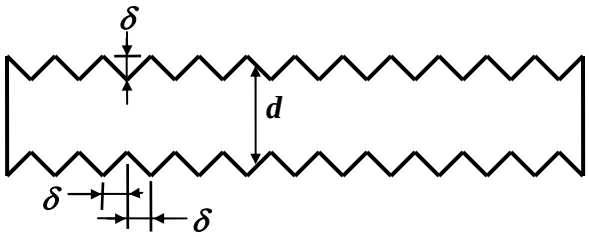

Fig 4.1 Schematic diagram of a silicon nanowire with a square cross section and four V-grooved side surfaces

In order to investigate whether it is feasible to engineer nanowire surfaces to reduce k below $k_{diffuse}$, we employ Monte Carlo (MC) simulation to verify our speculation of phonon backscattering by the idealized V-shape surfaces of a Si nanowire with a square cross section shown in Fig. 4.1. The nanowire size is chosen to be 22 nm because a previous measurement of a Si nanowire of this diameter yielded k much lower than $k_{diffuse}$ (Li et al. 2003). Note that this nanowire diameter is still much larger than λ_0 for most of the temperature range of the measurement so that the bulk phonon dispersion should be still applicable. Our MC simulation results reveal that the thermal conductivity of the nanowire with symmetric sawtooth or V-shape surface roughness can indeed be reduced below $k_{diffuse}$ when the V-groove height δ is increased to be larger than 0.5 nm.

4.2 SIMULATION METHOD

The Boltzmann equation for phonon transport in the presence of a temperature gradient is written as

$$\vec{V}_g \bullet \nabla T \frac{dN}{dT} = (\frac{\partial N}{\partial t})_c \tag{4.3}$$

where $\vec{V}_g$ is the group velocity

$$\vec{V}_g = \nabla_{\vec{q}} \omega \tag{4.4}$$

N is the distribution function, q is the phonon wavevector, T is the local temperature, ω is the phonon frequency, and $(\frac{\partial N}{\partial t})_c$ is the rate of change of N due to collisions. On the left side of Eq. (4.3), N can be replaced by N_0, the equilibrium Planck distribution. Consequently Eq. (4.3) can be read as

$$\vec{V}_g \bullet \nabla T \frac{dN_0}{dT} = \sum_{K'} [\Phi(q,q')N(q') - \Phi(q',q)N(q)] \tag{4.5}$$

where

$$N_0 = \frac{1}{\exp(\hbar\omega / k_B T) - 1} \tag{4.6}$$

Here $\hbar$ is Planck's constant divided by 2π, k_B is Boltzmann's constant, and $\Phi(q,q')$ is the function describing the scattering rate from state q' to state q, which depends on the phonon frequency and polarization.

Equation (4.5) is a nonlinear integro-differential equation. The transition rate $\Phi(q,q')$ on the right side of Eq. (4.5) is very complicated, and without simplification the formulation is difficult to solve. This difficulty can be avoided by using MC. To calculate thermal transport, MC does not try to solve Eq. (4.5) directly, but instead, follows a large number of phonons in a three-dimensional space subjected to a temperature gradient. The simulation domain is divided into many cells and initial local

temperature is imposed on each cell according to the temperature gradient. The initial velocity, polarization, and frequency of phonons are based on local temperatures. The number of phonons in each cell depends on the local temperature and the cell volume. For silicon, the frequency range between zero and the maximum cutoff frequency of the longitudinal acoustic branch is discretized into 1000 spectral intervals. The number of phonons per unit volume in the i^{th} spectral interval is calculated from the equilibrium Planck distribution

$$N_i = < n(\omega_{0,i}, LA) > D(\omega_{0,i}, LA)\Delta\omega_i + 2 < n(\omega_{0,i}, TA) > D(\omega_{0,i}, TA)\Delta\omega_i \qquad (4.7)$$

where $n(\omega_{0,i}, LA)$ and $n(\omega_{0,i}, TA)$ are the Bose-Einstein distribution for the longitudinal and transverse acoustic branches, respectively, $D(\omega_{0,i})$ is the density of states, and $\Delta\omega = \omega_{\max,LA} / N_b$, in which N_b is the number of intervals from zero to the maximum cutoff frequency of the longitudinal acoustic branch. In Eq. (4.7), three acoustic branches in the phonon dispersion relation are taken into account, i.e. one longitudinal acoustic branch and two transverse acoustic branches. Optical phonons are not considered because they contribute little to thermal conductivity due to their small group velocity. In this paper N_b is selected to be 1000. The total number of phonons can be obtained by summing up the phonons in the 1000 spectral intervals:

$$N = \sum_{i=1}^{N_b} N_i \qquad (4.8)$$

The actual number of phonons per unit volume calculated from Eq. (4.8) is usually a very large number. With the current computational power, it is impossible to simulate the movements of such a large number of phonons in each cell. In order to save

computation time, a prescribed number of phonons are used to represent the actual phonons in each cell by introducing a scaling factor:

$$W = \frac{N_{actual}}{N_{prescribed}} \tag{4.9}$$

Equation (4.9) indicates that one phonon in the simulation code will stand for W actual phonons.

Once the phonons are produced, the simulation starts with all of the phonons in given initial conditions with appropriate sampled frequencies, group velocities, wavevectors, and polarizations. A duration of free flight is set and all of the phonons move linearly from initial positions to new positions such that

$$\vec{r}_i = \vec{r}_{0,i} + \vec{V}_{g,i}\Delta t \tag{4.10}$$

where $\vec{r}_i, \vec{r}_{0,i}$ are the new and initial positions of the i^{th} phonon, respectively, and Δt is the free flight time. The free flight time is kept constant during the simulation and its value should be set as small as possible in order not to miss any scattering events. However, smaller Δt increases computation expense. To avoid undue computation burden, the time step in our simulation was set as one half of the smallest phonon scattering time.

The phonon scattering time was evaluated from Table 4.1. It was found that this time step gave stable simulation results. If the phonon encounters a boundary during free flight, it is reflected as described in Section 4.3.1. If it does not, the phonon lifetime is calculated according to Matthiessen's rule

$$\frac{1}{\tau_T} = \frac{1}{\tau_i} + \frac{1}{\tau_U} + \frac{1}{\tau_N} \tag{4.11}$$

where the total phonon lifetime τ_T depends on the lifetime for impurity scattering τ_i, the lifetime for U processes τ_U, and the lifetime for N processes τ_N. Each phonon has its own unique lifetime based on its frequency, polarization, impurity scattering time scale and local temperature (Holland 1963).

Table: 4.1: Parameters used in Monte Carlo simulation

Scattering process	Inverse relaxation time	parameter	
Impurity scattering	$\tau_i^{-1} = B_i \omega^4 \quad (s^{-1})$	B_i	$5.32 \times 10^{-46} \quad (s^3)$
Three phonon			
N process			
Transverse	$\tau_N^{-1} = B_{TN} \omega T^4 \quad (s^{-1})$	B_T	$9.3 \times 10^{-13} \ (\deg^{-4})$
Longitudinal	$\tau_N^{-1} = B_L \omega^2 T^3 \quad (s^{-1})$	B_L	$1.0 \times 10^{-30} \ (\deg^{-3} s)$
U process			
Transverse	$\tau_{TU}^{-1} = \begin{cases} 0 & (\omega < \omega_{12}) \\ B_{TU} \omega^2 / \sinh(\frac{\hbar \omega}{k_B T}) & (\omega \geq \omega_{12}) \end{cases} \quad (s^{-1})$	B_{TU}	$5.50 \times 10^{-30} \ (s)$
Longitudinal	$\tau_{LU}^{-1} = B_L \omega^2 T^3 \quad (s^{-1})$	B_L	1.0×10^{-30} $(\deg^{-3} s)$

The calculation of these lifetimes is discussed in more detail in the following sections. $P(t)$, the probability that a phonon has already existed for a free flight time Δt without being scattered, decreases in time such that

$$\frac{\partial P}{\partial t} = -\frac{P}{\tau_T} \tag{4.12}$$

The probability that the phonon is scattered after the free flight time is

$$\overline{P} = 1 - P = 1 - \exp(-\Delta t / \tau_T) \tag{4.13}$$

To impose a statistical scattering mechanism on the phonon, a random number R is generated. If $R < \overline{P}$, the phonon will be scattered and replaced by a new phonon at a different state. Then the new phonon begins its new free flight. If $R > \overline{P}$, the phonon will continue its free flight with its state unchanged. If the simulation time is long enough, the system equilibrates, and the final results can be extracted through averaging over a fixed time step (Mazumder and Majumder 2001).

When $R < \overline{P}$, a scattered phonon is found, then, the following procedure is used to determine which scattering process the phonon engaged in. As described in Eq. (4.11), three scattering processes constitute the transition rate. However, in fact, the phonon can only engaged in one of them. In order to distinguish which process the phonon engaged in, the phonon lifetime is divided into two parts,

$$\frac{1}{\tau_T} = \frac{1}{\tau_1} + \frac{1}{\tau_2} \tag{4.14}$$

where

$$\frac{1}{\tau_1} = \frac{1}{\tau_i} \tag{4.15}$$

and

$$\frac{1}{\tau_2} = \frac{1}{\tau_N} + \frac{1}{\tau_U} \tag{4.16}$$

The probability that the phonon engaged in impurity scattering process can be expressed as

$$P_i = \frac{1/\tau_1}{1/\tau_T} \tag{4.17}$$

A random number R_i is generated. If $R_i < P_i$, the phonon will be scattered by impurities. Otherwise, it engaged in three phonon scattering process. The same approach is used to determine if the phonon is engaged in N or U scattering processes.

4.3 SCATTERING MECHANISMS AND THEIR REALIZATION IN MC SIMULATIONS

4.3.1 Boundary scattering

During phonon transport, the primary phonon scattering processes are phonon-boundary collisions, impurity scattering, and three-phonon inelastic interactions. Boundary collisions play an important role in thermal resistance as the structure size decreases to nanoscale. When a phonon strikes the structure wall, a random number is first drawn. If this random number is less than a prescribed specularity parameter d, the phonon is specularly reflected using the following equation (Mazumder and Majumder 2001):

$$\vec{s}_r = \vec{s}_i + 2\left|\vec{s}_i \bullet \vec{n}\right|\vec{n} \tag{4.18}$$

where $\vec{s}_i, \vec{s}_r$ are the direction vectors of the incident and reflected phonons and $\vec{n}$ is the unit surface normal. In this case the phonon incident angle is equal to the reflected angle.

If the random number is larger than d, the phonon is reflected diffusely at the surface. Its direction is selected according to the following relation

$$\vec{s}_r = \sin\theta\cos\varphi\vec{t}_1 + \sin\theta\sin\varphi\vec{t}_2 + \cos\theta\vec{n} \tag{4.19}$$

where $\varphi = 2\pi R_2, \cos\theta = 2R_1 - 1$, R_1, R_2 are random numbers, $\vec{t}_1, \vec{t}_2$ are unit surface tangents which must be perpendicular to each other such that

$$\vec{t}_1 \times \vec{t}_2 = \vec{n} \tag{4.20}$$

If d is set to 1, the boundary is perfectly smooth and all phonons will be specularly reflected. In this case, the boundary scattering process does not contribute to thermal resistance.

4.3.2 Impurity scattering

Impurity scattering can be the dominant phonon scattering mechanism at low temperatures. The time scale for scattering by impurities is expressed using a simple model by Vincenti and Kruger (Vincenti and Kruger 1977):

$$\tau_i^{-1} = \alpha\sigma\rho\left|\vec{V}_g\right| \tag{4.21}$$

where α is a constant of order unity, ρ is the defect density per unit volume, and σ is the scattering cross-section expressed as (Majumder 1993)

$$\sigma = \pi r^2 \left(\frac{\chi^4}{\chi^4 + 1}\right) \tag{4.22}$$

Here r is the atomic radius of the impurity and $\chi = r|\vec{q}|, \vec{q}$ is the phonon wavevector. If only the isotope scattering is taken into account, Eq. (4.21) can be simplified as

$$\tau_i^{-1} = B_i \omega^4 \tag{4.23}$$

If a phonon is scattered by an impurity or a defect, its wavevector will be perturbed and its flight direction will be changed. In order to simulate the impurity scattering process, a new wavevector and a new velocity direction will be generated based on the phonon's frequency. The phonon frequency and polarization keep their original values.

4.3.3 Normal and Umpklapp scattering

Different expressions for three-phonon scattering rates have been adopted in literatures. Here we choose to use the expressions given by Holland (Holland 1963) because for bulk Si, extremely good fitting has been achieved with these expressions. The N and U scattering rates for transverse and longitudinal acoustic phonons are given as

$$\tau_L^{-1} = B_L \omega^2 T^3 \tag{4.24}$$

$$\tau_{TN}^{-1} = B_{TN} \omega T^4 \tag{4.25}$$

$$\tau_{TU}^{-1} = \begin{cases} 0 & (\omega < \omega_{12}) \\ B_{TU} \omega^2 / \sinh(\dfrac{\hbar\omega}{k_B T}) & (\omega \geq \omega_{12}) \end{cases} \tag{4.26}$$

Equation (4.26) gives the inverse lifetime for longitudinal phonons engaged in the N and U scattering processes. For transverse phonons the U scattering processes do not begin until $\omega \geq \omega_{12}$, where ω_{12} is the transverse branch phonon frequency corresponding to $K / K_{\max} = 0.5$. The parameters B_L, B_{TN}, B_{TU} in these equations are listed in Table 4.1.

4.4 SIMULATION SETUP

We have modeled the thermal conductivity of the silicon nanowire with symmetric sawtooth or V-shaped surface roughness of different sizes (δ) varied from 0.2 nm to 4 nm, with each side surface of the V grooves assumed to be either specular or diffuse. For comparison, we have also modeled a flat and diffuse case, where the details of surface roughness was ignored and all the nanowire surfaces were treated to be flat with phonon scattering by the flat surfaces assumed to be completely diffuse. For the simulations, the nanowire length was kept at 40 microns, and the average cross section at 22 nm x 22 nm.

The silicon nanowire was divided into 20 individual cells. The time step used in a MC simulation should be smaller than the smallest scattering time scale to avoid missing a scattering process. In our simulation, the time step was chosen in such a way that during the time step interval, the distance traveled by the fastest phonons is about half of the size of the simulation cell. In addition, the length of the simulation domain should be much longer than the phonon mean free path. If the length scale is comparable to or smaller than that, we found temperature jumps at the two ends of the nanowire. Similar effect was also reported by Chen et al. (Chen et al. 2005). The total number of steps used for all the simulation cases was 8×10^5, which was found to be long enough to stabilize the temperature. For the thermal conductivity simulations reported here, the values of the effective thermal flux in each cell were all within ten percent of the averaged flux and the temperature profiles were close to being linear. Hence, our simulation results satisfy two criteria, namely (i) the effective thermal flux in each simulation cell is nearly the same, and (ii) the temperature profile is reasonably close to linear. Note that the temperature

profiles should not be expected to be completely linear, since the thermal conductivity is temperature dependent.

4.3 SIMULATION RESULTS AND DISCUSSIONS

Figure 4.2(a) shows the temperature profile of a 40 micron long nanowire. The left end was kept at a constant temperature of 110 K and the right end at 100 K. The nanowire had a V-shape surface roughness of 2 nm. Figure 4.2(b) shows the temperature profile for the same nanowire with the left end kept at 305 K and right end at 295 K. Both Fig. 4.2(a) and 4.2(b) are quite linear. Fig. 4.2(a) shows higher slope at boundaries. This was also found to be true at lower temperatures. Chen et al. (2005) also reported similar effect. This is attributed to the fact that at lower temperature the mean free path of phonon is quite long and can be comparable to the length of the nanowire. This causes more phonon scattering at the two ends of the nanowire at lower temperature, thus a steeper drop.

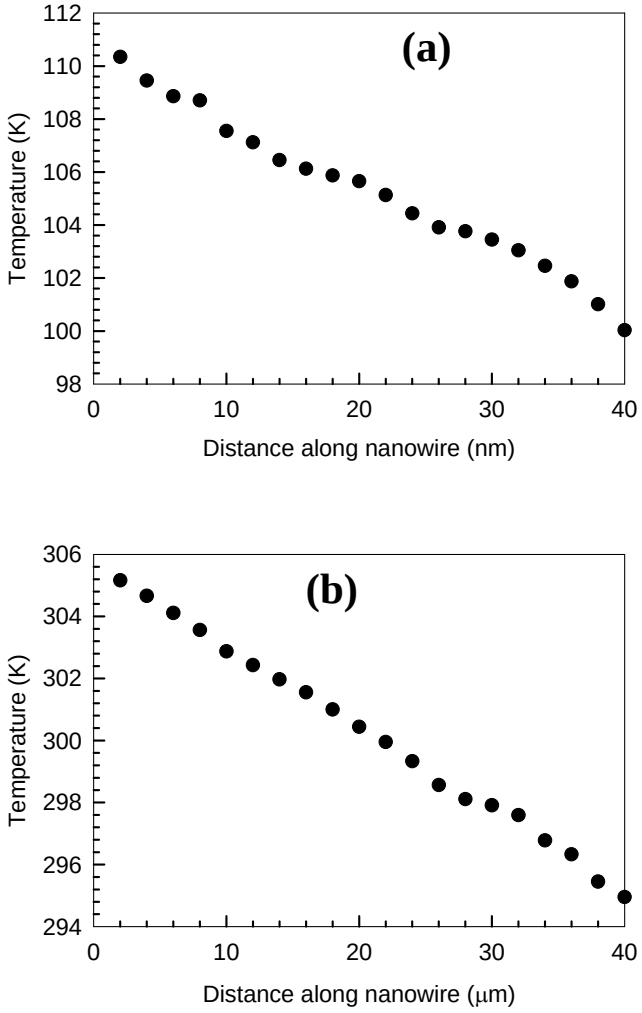

Fig. 4.2(a) Temperature profile along a 40 micron long silicon nanowire with an average square cross-section of 22 nm x 22 nm and a surface roughness of 2 nm. The left end is kept at 110 K and the right end kept at 100 K. (b) The temperature profile of the same wire with the left end kept at 305 K and the right end kept at 295 K.

In Fig. 4.3, we have plotted the thermal conductivity of the silicon nanowire at different temperatures for various surface roughness values. Also plotted are the thermal conductivity calculated for the flat and diffuse case, the experimental thermal conductivity data of a 22 nm diameter silicon nanowire, the MC simulation results of

Chen et al. of a 22 nm diameter nanowire, and the theoretical calculation of thermal conductivity of silicon nanowire by Prasher (Prasher 2006). Prasher's calculations were based on grey medium approximation.

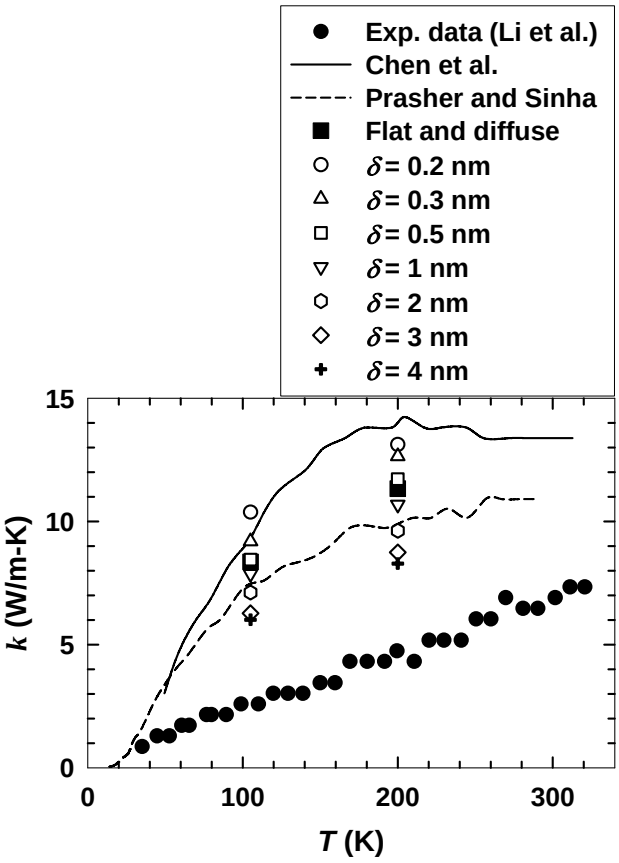

Fig. 4.3:Thermal conductivity of a 40 micron long silicon nanowire with average square cross-section of 22 nm x 22 nm for various temperatures for various surface roughness. Surface is treated specular. Also plotted are the experimental thermal conductivity data (Li et al. 2003), the MC simulation data from Chen et al. 2005, and the theoretical calculation results from Prasher (Prasher 2006).

The thermal conductivity obtained by the MC simulation for the flat and diffuse case is 8.3, 11.3, and 12.35 W/m-K, respectively, for temperature 105, 200, and 300 K. These values are essentially k_{diffuse}, and are considerably higher than Li et al.'s

measurement values of 2.6, 4.7, and 6.9 W/m-K near the three temperatures (Li et al. 2003). As shown previously by Chen et al., and Prasher, the difference between their calculation results and the experimental data of a 22 nm Si nanowire is significant (Chen et al. 2005; Prasher 2006). The modification of the phonon dispersion relation due to finite size of the wire can lead to a reduction in the effective group velocity of phonons in a nanowire; however, this is unlikely the reason because the discrepancy between the data and the model occurred at high temperatures, where the dominant phonon wavelength is well below 1 nm and much smaller than the diameter of the nanowire. The phonon dispersion can be altered due to size confinement only when the phonon wavelength is comparable to the diameter of the nanowire.

Figure 4.3 shows that the thermal conductivity values for different surface roughness values are lower than the flat and diffuse case at temperature 105 and 200 K. In Fig. 4.4, we have plotted k of the symmetric sawtooth surfaces of different δ values.

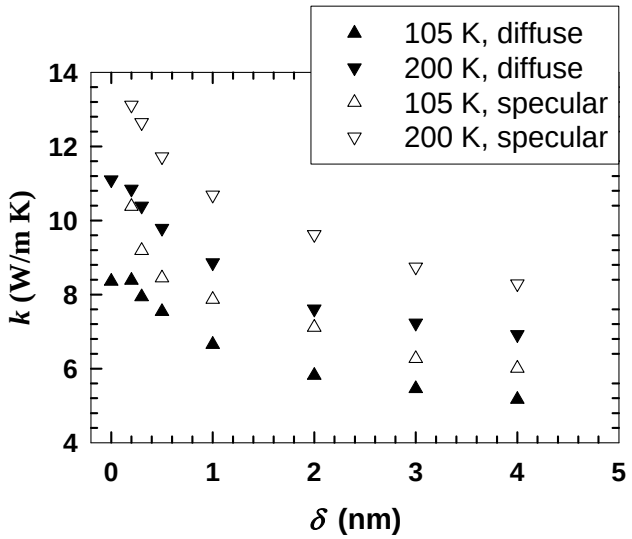

Fig. 4.4: Thermal conductivity of a 40 μm long silicon nanowire with either specular (unfilled symbols) or diffuse (filled symbols) sawtooth surfaces and average square cross-section of 22 nm x 22 nm as a function of V groove height (δ).

For specular sawtooth surfaces, at $\delta \approx 0.5$ nm k is close to $k_{diffuse}$, and decreases with increasing δ to be below $k_{diffuse}$ for $\delta > 1$ nm. For diffuse sawtooth surfaces with different δ values, k is smaller than $k_{diffuse}$ and lower than the corresponding thermal conductivity for the specular sawtooth surfaces. While $k_{diffuse}$ is the lowest possible thermal conductivity of a nanowire with randomly-distributed surface roughness that scatter phonons completely diffusely, the observed $k<k_{diffuse}$ is caused by the net backscattered phonon component on the sawtooth surface.

We want to emphasize that as the V-groove height δ is varied, the volume of the nanowire is constant and thus the effective diameter is kept the same. To further confirm that the observed thermal conductivity reduction below $k_{diffuse}$ is indeed due to phonon backscattering instead of an effective reduction of the nanowire diameter, we have used the MC method to show that thermal rectification can occur in nanowires with

asymmetric sawtooth surface roughness. As shown in Fig. 4.5, the net heat current is different when the temperatures at the two ends of the nanowire with asymmetric sawtooth surface roughness are exchanged.

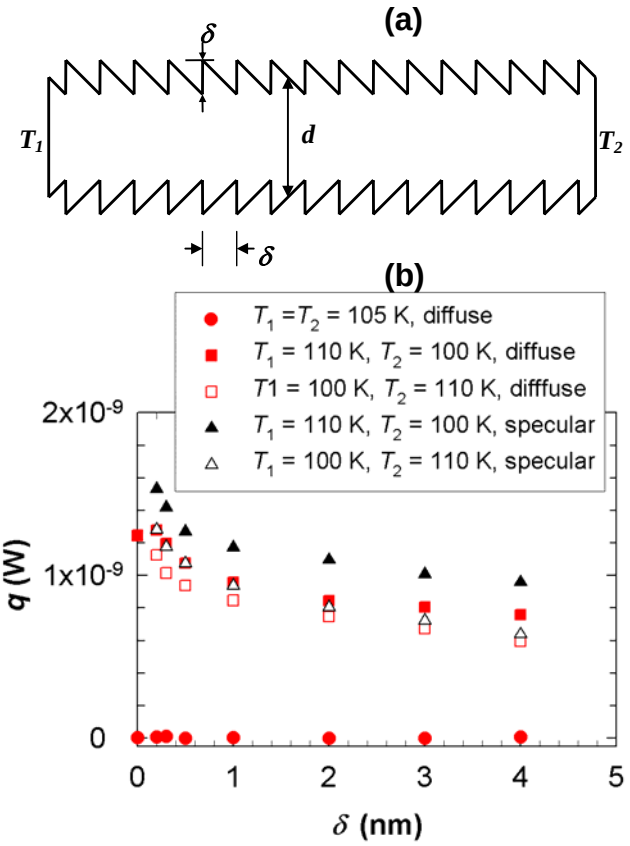

Fig 4.5: (a) Schematic diagram of a silicon nanowire with a square cross section and four side surfaces of asymmetric sawtooth roughness. (b) Net heat current as a function of sawtooth height (δ) for different end temperatures T_1 and T_2 for either diffuse or specular side surfaces of the saw-teeth.

Here, the heat current rectification is due to different degrees of backscattering of phonons by the two asymmetric surfaces of the each sawtooth. The rectification effect is larger when the sawtooth surface is specular than when it is diffuse. Note that the net heat

current from the MC simulation is zero when the two ends of the nanowire are kept at the same temperature, suggesting that the MC results satisfy the second law of thermodynamics.

Ziman's formula in Eq. 4.2 can only give p in the range between 0 and 1 for random surface roughness that obtains a Gaussian distribution. Consequently, it can only account for the diffuse and specular (or forward scattered) components of phonons scattered by a surface, and fails to describe the backscattered component which can be dominant under certain conditions such as the sawtooth surface roughness. Analogous to the partially diffuse and partially specular surface that is described by $0 < p < 1$, a partially diffuse and partially backscattering surface needs to be described with negative p in the range between 0 and -1. This will allow l_B to be lower than the nanowire diameter obtained for the diffuse limit of $p = 0$. Similar to the upper limit of $p = 1$ for purely specular forward scattering, the lower limit of $p = -1$ correspond to complete backscattering of phonons by the V-grooved surfaces, which makes the mean free path zero resulting in zero thermal conductivity.

By treating the V-grooved surfaces of the 22 nm diameter Si nanowires as geometrically flat and partially diffuse, partially backscattering surface that is described by $0< p <-1$, we have calculated the thermal conductivity using MC simulation. The results are shown in Fig. 4.6.

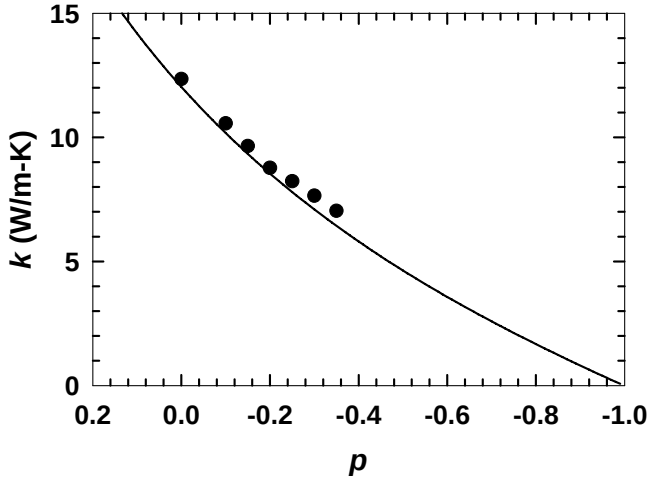

Figure 4.6. Thermal conductivity of a 22 nm diameter silicon nanowire where the surfaces are treated as geometrically flat and characterized by specularity parameter *p*. Filled circles are the MC calculation results. The solid line is obtained using Eq. (4.29).

Also shown in Fig. 4.6 are the results from an analytical model described below. This model obtains l_B using Eq. (4.1), with both positive and negative *p*. The effective phonon-boundary scattering mean free time was obtained according to

$$\tau_B(P,\omega) = l_B / v_{p,\omega} \tag{4.27}$$

where $v_{p,\omega}$ is the velocity of phonons of frequency ω and phonon polarization *P*. The effective scattering mean free time accounting for different scattering mechanisms was calculated according to the Matthiessen's rule

$$\frac{1}{\tau_{eff}} = \frac{1}{\tau_i} + \frac{1}{\tau_U} + \frac{1}{\tau_N} + \frac{1}{\tau_B} \tag{4.28}$$

where τ_i, τ_U, and τ_N are the scattering mean free time for impurity, Umklapp, and Normal scattering process, respectively. The thermal conductivity was calculated as (Callaway 1959; Holland 1963):

$$k = \frac{1}{3}\sum_{P}\int_{0}^{\omega_{\max}} c_{\omega} v_{p,\omega}^{2} \tau_{eff}\, d\omega \tag{4.29}$$

In Eq. (4.29), $v_{p,\omega}$ is the phonon group velocity and c_{ω} is the frequency dependent specific heat given by

$$c_{\omega} = \frac{\partial}{\partial T}\left(\frac{1}{\exp(\hbar\omega / k_b T) - 1}\right)\hbar\omega \times D(\omega) \tag{4.30}$$

where $D(\omega)$ is the density of states per unit volume, $\hbar$ is the Planck's constant, and k_b is the Boltzmann constant.

The phonon dispersion relation used to calculate the thermal conductivity was the experimental dispersion curve obtained by Brockhouse (Brockhouse 1959), which was discretized into 1000 intervals for integral calculation. The thermal conductivity of a 22 nm diameter silicon nanowire was calculated based on Eq. (4.29) at temperature 300 K and for various p ranging from positive to negative values. As shown in Fig. 4.6, the analytical approach is in very good agreement with the MC simulation, both showing a decreasing k with decreasing p.

By matching the k obtained by MC at 300 K for the V-grooved surfaces with those obtained by MC and the analytical approach (Eq. (4.29)) for geometrically flat surfaces, we have determined the corresponding p values if the V-grooved surfaces are assumed to be flat surfaces characterized by specularity p. The obtained p as a function of δ is shown in Fig. 4.7.

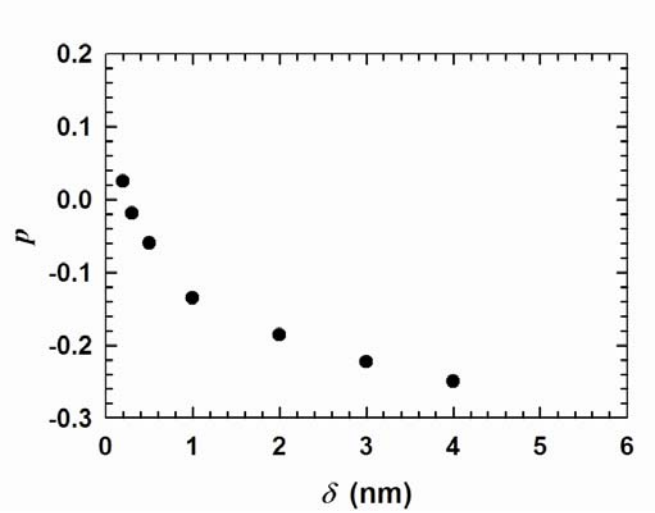

Fig. 4.7: The corresponding specularity (p) of the V-grooved surface as a function of the groove height (δ) if the specular V-grooved surfaces are treated as geometrically flat with random surface roughness characterized by p. The filled circles are the results obtained by matching k from Fig. 4.5 with those of Fig. 4.6 for specular V-grooved surfaces.

For δ of about 0.25 nm, a roughness comparable to atomic corrugation, p already reaches a value of 0 corresponding to totally diffuse scattering. This is still consistent with Ziman's formula in Eq. 2. However, as δ increases further, p decreases to a negative value instead of saturating at 0 following Ziman's formula. The negative p originates from phonon backscattering that is not properly treated in Ziman's formula.

4.4 CONCLUSIONS

The Monte Carlo simulation reveals that certain types of surface roughness such as the sawtooth on a nanowire can lead to phonon backscattering and suppress the thermal conductivity below the diffuse surface limit. Phonon backscattering on asymmetric sawtooth surface roughness can further cause thermal rectification. Ziman's formula for surface specularity p serves as the basis of various previous modeling efforts

on phonon transport in nanowires and thin films. Because Ziman's formula can only obtain surface specularity parameter in the range of 0 and 1 for random surface roughness that obtains a Gaussian distribution, it can only account for the diffuse and specular components of scattered phonons, and is inadequate to describe the backscattered component that can be dominant at certain rough surfaces such as the sawtooth surfaces. We suggest that this problem can be addressed by introducing an extended p range between -1 and 1, where $-1<p<0$ describes partially diffuse and partially backscattering and $0<p<1$ results in partially diffuse and partially specular scattering. Most importantly, the MC simulation results show that surface roughness can be engineered to facilitate phonon backscattering so that the diffuse surface limit of nanowire thermal conductivity can be beaten. In the n-type leg of a thermoelectric device, moreover, the net phonon flux direction is opposite to the electron flux direction. For an n-type nanowire, therefore, one can potentially employ an asymmetric surface roughness to reduce phonon conductivity primarily along one direction with much less reduction in the electron conductivity along the opposite direction, potentially increasing the ZT.

Chapter 5 Conclusions

NEMD simulation method was employed to model the temperature distribution and thermal resistance of a nanoscale point constriction formed between two silicon substrates. The radius of the heated zone in the cold substrate was found to approach a limit of 20 times the average nearest-neighbor distance of impurity doping atoms when the constriction radius is reduced below the inter-dopant distance. The phonon mean free path at the constriction was found to be suppressed by diffuse phonon-boundary scattering and phonon-impurity scattering. When the constriction radius is larger than 1 nm, the MD thermal resistances of the constriction are close to the ballistic thermal resistance, suggesting that surface reconstruction does not reduce the phonon transmission coefficient at the constriction significantly. When the constriction radius is 0.5 nm, however, the MD result is considerably lower than the ballistic resistance calculated based on bulk phonon dispersion. The MD resistance increases slightly with decreasing specularity or increasing doping concentration due to the increase in the diffusive resistance.

The NEMD method is further employed to calculate the temperature distribution and thermal resistance at nanoscale line constrictions formed between two silicone substrates. Similar to the nano point constriction, the thermal resistance at the nano line constriction is dominated by the nano line constriction for constriction half width in the range of 0.5 nm and 6 nm.

Monte Carlo simulation of phonon transport was performed in a Silicon nanowire with sawtooth surface roughness. Phonon backscattering was observed from the nanowire

surface suppressing the thermal conductivity below the diffuse surface limit. In addition, asymmetric sawtooth nanowire surfaces can further cause phonon rectification, making the axial thermal conductance of the nanowire direction dependent.

Bibliography

Abeles, B., D. S. Beers, et al. "Thermal Conductivity of Ge-Si Alloys at High Temperatures," *Physical Review* 125(1), 44 (1962).

Allen, M. P. and Tildesley D. J., Computer Simulation of Liquids. (Oxford, UK, Clarendon Press 1987)

Armstrong, B. H., "N Processes, the Relaxation-Time Approximation, and the Thermal Conductivity," *Phys. Rev. B* 32, 3381 (1985).

Asen-Palmer, M., Bartkowski, K., Gmelin, E., Cardona, M., Zhernov, A. P., Inyushkin, A. V., Taldenkov, A., Ozhogin, V. I., Itoh, K. M., and Haller, E. E., "Thermal Conductivity of Germanium Crystals with Different Isotopic Compositions," *Phys. Rev. B* 56, 9431 (1997).

Ashcroft, N. W. and Mermin N. D., Solid State Physics. (New York, Harcourt College Publishers 1976).

Asheghi, M., Kurabayashi, K., Kasnavi K., and Goodson, K. E., "Thermal conduction in doped single-crystal silicon films," *J. Appl. Phys.* 91, 5079 (2002).

Auld, B. A., *Acoustic Fields and Waves in Solids*, (Wiley, NY 1973).

Bachelli, L., and Jacoboni, C., "Electron-Electron Interactions in Monte Carlo Transport Calculations," *Solid State Commun.* 10, 71 (1972).

Bahadur, V., Xu, J., Liu, Y., Fisher, T.S., "Thermal Resistance of Nanowire-Plane Interfaces," *J. Heat Transfer* 127, 664 (2005)

Balandin, A., and Wang, K.L. “Significant Decrease of the Lattice Thermal Conductivity due to Phonon Confinement in a Free-standing Semiconductor Quantum Well,” *Physical Review B* 58(3), 1544 (1998).

Berman, A. S., Maegley, W. J., “Internal Rarefied Gas Flows with Backscattering,” *Phys. Fluids* 1972**,**15, 772.

Bhattacharya, P., Saha, S. K., Yadav, A., Phelan P., and Prasher, R. S., “Brownian dynamics simulation to determine the effective thermal conductivity of nanofluids,” *J. Appl. Phys.* 95, 6492 (2004).

Blencowe, M. P., “Quantum Energy Flow in Mesoscopic Dielectric Structures,” *Phys. Rev. B* 59, 4992 (1999).

Brockhouse, B. N., 1959, “Lattice Vibrations in Silicon and Germanium,” *Phys. Rev. Lett.*, 2, 256 (1959).

Budd, H., “Path Variable Formulation of the Hot Carrier Problem,” *Phys. Rev.*, 158, 798 (1967).

Cahill, D.G., Ford, W.K., Goodson, K.E., Mahan, G.D., Majumdar, A., Maris, H.J., Merlin. R., and Phillpot, S.R., “Nanoscale Thermal Transport,” *J. of App. Phys* 93,. 793 (2003)

Callaway, J., “Model of Lattice Thermal Conductivity at Low Temperatures,” *Phys. Rev.*, 113, 1046 (1959).

Chantrenne, P. and Barrat, J. L., “Finite Size Effects in Determination of Thermal Conductivities: Comparing Molecular Dynamics Results with Simple Models.” *Journal of Heat Transfer* 126, 577 (2004).

Che, J., T. Cagin, T., Deng W., and Goddard, W. A., J., "Thermal Conductivity of Diamond and Related Materials from Molecular Dynamics Simulations." *Journal of Chemical Physics* 113(16), 6888 (2000).

Chen Y.; Li, D.; Lukes, J.R.; Majumdar, A. “Monte Carlo Simulation of Silicon Nanowire Thermal Conductivity,” *J. Heat Transfer* 127, 1129 (2005).

Chen, G., “Ballistic-Diffusive Heat-Conduction Equations,” *Phys. Rev. Lett.*, 86, 2297 (2001).

Chen, G., “Size and Interface Effects on Thermal Conductivity of Superlattices and Periodic Thin-Film Structures,” *J. Heat Transfer* 119, 220 (1997).

Chen, G., “Thermal conductivity and ballistic-phonon transport in the cross-plane direction of superlattices,**”** *Phys. Rev. B* 57, 14958 (1998)

Chen, G; Shakouri, A. “Heat Transfer in Nanostructures for Solid-State Energy Conversion,” *J. Heat Transfer* 124, 242 (2002).

Choi, S.-H. and S. Maruyama “Evaluation of the Phonon Mean Free Path in Thin Films by Using Classical Molecular Dynamics” *Journal of the Korean Physical Society* 43(5), 747 (2003)

Chuang, H. F., Cooper, S. M., Meyyappan M., and Cruden, B. A., “Improvement of Thermal Contact Resistance by Carbon Nanotubes and Nanofibers,” *J. Nanoscience and Nanotech.* 4, 964 (2004)

Chuang, H. F., Cooper, S. M., x Meyyappan S. M., and Cruden, B. A., J., “Improvement of Thermal Contact Resistance by Carbon Nanotubes and Nanofibers,” *Nanoscience and Nanotech.* 4, 964 (2004)

Chung, J. D., A. J. H. McGaughey, et al.. “Role of Phonon Dispersion in Lattice Thermal Conductivity Modeling,” *Journal of Heat Transfer* 126: 376-380 (2004).

Cooper, M. G., Mikic B. B., and Yovanovich, M. M., “Thermal contact conductance,” *Int. J. Heat Mass Transfer* 12, 279 (1968).

Daly, B. C. and H. J. Maris. “Calculation of the Thermal Conductivity of Superlattices by Molecular Dynamics Simulation,” *Physica B* 316-317: 247 (2002).

Dames, C., and Chen, G., “Theoretical Phonon Thermal Conductivity of SI/Ge Superlattice Nanowires,” *J. Appl. Phys*., 95, 682 (2004).

Ding, K. and H. C. Andersen “Molecular-Dynamics Simulation of Amorphous Germanium,” *Phvsical Review B* 34(10), 6987 (1986).

Feng, X.-L., Z.-X. Li, et al. “Molecular Dynamics Simulation of Thermal Conductivity of Nanoscale Thin Silicon Films,” *Microscale Thermophysical Engineering* 7, 153 (2003).

Feng, X.-L., Z.-X. Li, et al.,. “Molecular Dynamics Study on Thermal Conductivity of Nanoscale Thin-Films,” *Chinese Science Bulletin* 46(7), 604 (2001).

Flik, M. I., B. I. Choi, et al. “Heat Transfer Regimes in Microstructures.” *Journal of Heat Transfer* 114: 666-674 (1992).

Frenkel, D. and B. Smit, Understanding Molecular Simulation from Algorithms to Applications. (New York, Academic Press 2001).

Friendman, R., S., McAlpine, M., C., Ricketts, D. S., Lieber, C. M., “Nanotechnology: High-speed integrated nanowire circuits,” *Nature* 434, 1085 (2005)

Glassbrenner C. J., and Slack, G. A., “Thermal Conductivity of Silicon and Germanium from 3°K to the Melting Point,”*Phys. Rev.* 134, A1058 (1964).

Goldberg, D. E., *Genetic Algorithms in Search, Optimization, and Machine Learning*, (Addison-Wesley Publishing Company 1982).

Han, Y.-J. and P. G. Klemens, "Anharmonic Thermal Resistivity of Dielectric Crystals at Low Temperatures," *Phvsical Review B* 48(9): 6033-6042 (1993).

Harman, H. F., Martin Y. C., and Wickramasinghe, H. K., "Thermally assisted recording beyond traditional limits," *Appl. Phys. Lett.* 84, 810 (2004).

Herring, C., "Role of Low Energy Phonons in Thermal Conduction," *Phys. Rev.*, 95, pp. 954–965 (1954).

Hirst, D. M.,. A Computational Approach to Chemistry. (Oxford London, Blackwell Scientific Publications 1990).

Holland, M. G. "Analysis of Lattice Thermal Conductivity," *Phvsical Review* 132(6): 2461-2471 (1963).

Hu X., *et al.* in *Proc SEMI-THERM, San Jose, CA, 2005.*

Jacoboni, C., "Noise and Diffusion of Hot Holes in Si," *Solid-State Electron.,* 21, 315–318 (1978).

Jacoboni, C., and Reggiani, L., "The Monte Carlo Method for the Solution of Charge Transport in Semiconductors with Applications to Covalent Materials," *Rev. Mod. Phys.*, 55, pp. 645–705 (1983).

Ju, Y. S. and K. E. Goodson, "Phonon Scattering in Silicon Thin Films with Thickness of Order 100 nm," *Applied Physics Letters* 74(20): 3005-3007 (1999).

Jund P., and Jullien, R., "Molecular-dynamics calculation of the thermal conductivity of vitreous silica," *Phys. Rev. B* 59, 13707 (1999).

Kelly F. X., and Ungar, L. H., "A molecular dynamics investigation of solute trapping during rapid solidification of silicon," *J. Cryst. Growth* 102, 658 (1990).

Khitun, A., and Wang, K. L., "Modification of the Three-Phonon Umklapp Process in A Quantum Wire," *Appl. Phys. Lett*., 79, pp. 851–853 (2001).

Kim, P., Shi, L., Majumdar, A., and McEuen, P.L., "Thermal Transport Measurements of Individual Multiwalled Nanotubes," *Phys Rev Lett*, 87, 215502 (2001).

Klemens, P. G., *Solid State Physics*, (Academic Press, NY 1958).

Klitsner, T., VanCleve, J. E., Fisher, H. E., and Pohl, R. O., "Phonon Radiative Heat Transfer and Surface Scattering," *Phys. Rev. B*, 38, 7576 (1988).

Kremer, R. K., Graf, K., Cardona, M., Devyatykh, G. G., Gusev, A. V., Gibin, Inyushkin, A. M., Taldenkov, A. N., and Pohl, H.-J., 2004, "Thermal Conductivity of Isotropically Enriched Si: Revisited," *Solid State Commun.*, 131, pp. 499–503 (2004).

Kurosawa, T., "Monte Carlo simulation of hot electron problems," *Proceedings of the International Conference on the Physics of Semiconductor*, Kyoto, J. Phys. Soc. Jpn. 21, pp. 424–427 (1966).

Lee, Y. H., Biswas, R., C. M. Soukoulis, C. Z. Wang, C. T. Chan and K. M. Ho, "Molecular-Dynamics Simulation of Thermal Conductivity in Amorphous Silicon," *Phys. Rev. B* 43, 6573 (1991).

Li, D., Wu, Y., Fan, R., Yang, P., and Majumdar, A., "Thermal Conductivity of Si/SiGe Superlattice Nanowires," *Appl. Phys. Lett*., 83, 3186 (2003).

Li, D.; Wu, Y.; Kim, P.; Shi, L.; Yang, P.; Majumdar, A., "Thermal Conductivity of Individual Silicon Nanowires," *Appl. Phys. Lett*. 83, 2934 (2003)

Li, X.-P., Chen, G., Allen P. B., and Broughton, J. Q., "Energy and vibrational spectrum of the Si(111) (7×7) surface from empirical potentials," *Phys. Rev. B* 38, 3331 (1988).

Lin, Y., Sun X., and Dresselhaus M. S., "Theoretical investigation of thermoelectric transport properties of cylindrical Bi nanowires," *Phys. Rev. B* 62, 4610 (2000).

Little, W. A., Can. J. Phys. 37, 334 (1959).

Liu, W. and M. Asheghi, "Phonon-Boundary Scattering in Ultrathin Single-Crystal Silicon Layers," *Applied Physics Letters* 84, 381 9 (2004).

Liu, W. and M. Asheghi, "Thermal Conduction in Ultra-Thin Pure and Doped Single Crystal Silicon Layers at High Temperatures,". 2005 ASME Summer Heat Transfer Conference, San Francisco, CA, USA (2005).

Liu, W. and M. Asheghi, "Thermal Modeling of Self-Heating in Strained-Silicon MOSEFTs,". Thermal and Thermomechanical Phenomena in Electronic Systems, Las Vegas, Nevada, USA (2004).

Lu, X., Chu, J. H., and Shen, W. Z., "Modification of the Lattice Thermal Conductivity in Semiconductor Rectangular Nanowires," *J. Appl. Phys.* 93, 1219 (2003).

Lukes, J. R., D. Y. Li, et al., "Molecular Dynamics Study of Solid Thin-Film Thermal Conductivity," *Journal of Heat Transfer* 122, 536 (2000).

Lyeo, H. K., Khajetoorians, A. A., Shi, L., Pipe, K. P., Ram, R. J., Shakouri A., and Shih, C. K., "Profiling the Thermoelectric Power of Semiconductor Junctions with Nanometer Resolution," *Science* 303, 816 (2004).

Madhusudana, C. V., *Thermal Contact Conductance*, (Springer-Verlag, New York, 1996), 1-43.

Maiti, A., Mahan G. D., and Pantelides, S. T., "Dynamical simulations of nonequilibrium processes - Heat flow and the Kapitza resistance across grain boundaries," *Solid State Commun.* 102, 517 (1997).

Majumdar, A., "Microscale Heat Conduction in Dielectric Thin Films," *ASME J. Heat Transfer*, 115, 7 (1993).

Matulionis, A., Pozela, J., and Reklaitis, A., "Monte Carlo Treatment of Electron-Electron Collisions," *Solid State Commun.*, 16, pp. 1133 (1975).

Mazumder, S., and Majumdar, A., "Monte Carlo Study of Phonon Transport in Solid Thin Films including Dispersion and Polarization," *ASME J. Heat Transfer* 123, pp. 749 (2001).

McGaughey, A. J. and M. Kaviany, "Quantitative Validation of the Boltzman Transport Equation Phonon Thermal Conductivity Model Under the Single-Mode Relaxation Time Approximation." *Phvsical Review B* 69, 094303 (2004).

McGaughey, A. J. H. and M. Kaviany "Molecular Dvnamics Calculations of the Thermal Conductivity of Silica Based Crystal," AIMASME Joint Thermophysics and Heat Transfer Conference, St. Louis, MO (2002).

McGee, G. E., Schankula, M. H., and Yovanovich, M. M., 1985, ''Thermal Resistance of Cylinder-Flat Contacts: Theoretical Analysis and Experimental Verification of a Line Contact Model,'' Nucl. Eng. Des., 86, pp. 369–381 (1985).

McQuarrie, D. A., Statistical Mechanics. (New York, Harper Collins 1976).

Miiller-Plathe, F., “A Simple Nonequilibrium Molecular Dynamics Method for Calculating the Thermal Conductivity,.” *Journal of Chemical Physics* 106(14): 6082-6085 (1997).

Mingo, N., “Calculation of Si Nanowire Thermal Conductivity using Complete Phonon Dispersion Relations,” Phys. Rev. B, 68, 113308 (2003).

Mingo, N., “Thermoelectric figure of merit and maximum power factor in III–V semiconductor nanowires,” *Appl. Phys. Lett.* 84, 2652 (2004)

Mingo, N., Yang, L., Li., D., and Majumdar, A., 2003, “Predicting the Thermal Conductivity of Si and Ge Nanowires,” *Nano Lett.*, 3, 1713 (2003).

Narumanchi, S. V. J. (2003). Heat Transport in Sub-micron Conduction. Mechanical Engineering. Pittsburgh, Ph.D. thesis, Carnegie Mellon University.

Narumanchi, S. V. J., J. Y. Murthy, et al. (2003). "Simulation of Unsteady Small Heat Source Effects in Sub-micron Heat Conduction." *ASME Journal of Heat Transfer* 125(5): 896-903 (2003).

Narumanchi, S. V. J., J. Y. Murthy, et al. (2004). "Submicron Heat Transport Model in Silicon Accounting for Phonon Dispersion and Polarization." *ASME J. Heat Transfer*, 126(6)**:** 946-955 (2004).

Ngo, Q., Cruden, B. A., Cassell, A. M., Sims, G., Meyyappan, M., Li, J., Yang, C. Y., “Thermal Interface Properties of Cu-filled Vertically Aligned Carbon Nanofiber Arrays,” *Nano Lett.* 4, 2403 (2004).

Nikolic B., and Allen, P. B., “Electron transport through a circular constriction,” *Phys. Rev. B* 60, 3963 (1999).

Peierls, R. E., 1955, *Quantum Theory of Solids*, (Oxford University Press, Oxford 1955).

Peng, H., Meister, S., Chan, C. K., Zhang, X. F., Cui, Y., "Morphology Control of Layer-Structured Gallium Selenide Nanowires," *Nano Letters* 7, 199 (2007).

Peterson, R. B., 1994, "Direct Simulation of Phonon-Mediate Heat Transfer in A Debye Crystal," *ASME J. Heat Transfer*, 116, 815–822 (1994).

Pop, E., S. Sinha, Goodson K. E., "Monte Carlo Modeling of Heat Generation in Electronic Nanostructures," International Mechanical Engineering Conference and Exposition, New Orleans, Louisiana (2002).

Prasher, R. S., "Ultralow thermal conductivity of a packed bed of crystalline nanoparticles: A theoretical study," *Phys. Rev. B.*74, 165413 (2006)

Prasher, R. S., Tao, T., Majumdar, A., Proceedings of International Mechanical Engineering Congress and Exposition, IMECE2006-15592 (2006)

Prasher, R.S., "Predicting the Thermal Resistance of Nanosized Constrictions" *Nano Lett.* 5, 2155 (2005)

Prasher, R.S., Shipley, J., Prstic, S., Koning, P., and Wang, J-L., "Thermal Resistance of Particle Laden Polymeric Thermal Interface Materials," *J. of Heat Transfer* 125, 1170 (2003)

Rapaport, D. C., "The Art of Molecular Dynamics Simulation", Cambridge University Press, 2004.

Ross, F. M., Tersoff, J. and Reuter M. C., "Sawtooth Faceting in Silicon Nanowires," *Phys. Rev. Lett.* 95, 146104 (2005)

Saha S. and Shi L., “Molecular Dynamics Simulation of Thermal Transport at a Nanometer Scale Constriction in Silicon,” *J. Appl. Phys.*101, 074304 (2007)

Saha S., Shi L., “Molecular Dynamics Simulation of Thermal Transport at a Nanometer Size Point Contact on a Planar Silicon Substrate,” Proceedings of 2005 Summer Heat Transfer Conference, HT2005-72308 (2005)

Saha S., Shi L., Prasher R., “Monte Carlo Simulation of Phonon Backscattering in a Nanowire,” Proceedings of 2006 Int. Mech. Eng. Congress & Exp, IMECE2006-15668: 1-5 (2006)

Schelling, P. K., S. R. Phillpot, Keblinski P., “Comparison of Atomic-Level Simulation Methods for Computing Thermal Conductivity,” *Physical Review B* 65: 144306 (2002).

Sharvin, Y. V., Sov. Phys. JETP **21**, 655 (1965).

Shi, L.; Hao, Q.; Yu, C.; Mingo, N.; Kong, X.; Wang, Z.L., “Thermal conductivities of individual tin dioxide nanobelts,” *Appl. Phys. Lett.*, 84, 2638 (2004).

Simons, S., “On the Mutual Interaction of Parallel Phonons,” *Proc. Phys. Soc. London*, 82, 401 (1963).

Sinha, S., P. K. Schelling, Goodson K. E., “Atomistic Simulations of Non-equilibrium Phonons in Nanotransistors,” SRC-TECHCON, Dallas, TX (2003).

Slack, G. A., “Thermal Conductivity of Pure and Impure Silicon, Silicon Carbide, and Diamond,**”** *J. Appl. Phys.* 35, 3460 (1964).

Stillinger F. H., and Weber, T. A., “Computer simulation of local order in condensed phases of silicon,” *Phys. Rev. B* 31, 5262 (1985).

Sverdrup, P. G., Y. S. Ju, Goodson K. E., "Sub-Continuum Simulations of Heat Conduction in Silicon-on-Insulator Transistors," *Journal of Heat Transfer* 123, 130 (2001).

Tamura, S.-I., Y. Tanaka, Maris H. J.**, "**Phonon group velocity and thermal conduction in superlattices," *Physical Review B* 60, 2627 (1999).

Vincenti, W. G., and Kruger, C. H., 1977, *Introduction to Physical Gas Dynamics* (Robert Krieger Publication, New York 1977).

Volz, S. G. and G. Chen**,** "Lattice Dynamic Simulation of Silicon Thermal Conductivity," *Phvsica B* 263, 709 (1999).

Volz, S. G. and G. Chen**,** "Molecular-Dynamics Simulation of Thermal Conductivity of Silicon Crystals," *Physical Review B* 61(4): 2651-2656 (2000).

Volz, S., and Chen, G., "Molecular Dynamics Simulation of Thermal Conductivity of Silicon Nanowires," *Appl. Phys. Lett.*, 75, pp. 2056–2058 (1999).

Volz, S., J. B. Saulnier, et al.**, "**Computation of Thermal Conductivity of SiGe Superlattice by Molecular Dynamics Technique," *Microelectronics Journal* 31, 815 (2000).

Volz, S., Lemonnier, D., and Saulnier, J.-B., "Clamped Nanowire Thermal Conductivity Based on Phonon Transport Equation," *Microscale Thermophys. Eng.*, **5**, pp. 191–207 (2001).

Weber, L., Gmelin E., and Queisser, H. J., "Thermal resistance of silicon point contacts," *Phys. Rev. B* 40, 1244 (1989).

Wexler, G., "The size effect and the non-local Boltzmann transport equation in orifice and disk geometry," *Proc. Phys. Soc. London* 89, 927 (1966).

Xu, J. and Fisher, T.S., *International Mechanical Engineering Congress and Exposition, Anaheim, CA, Nov. 13-20*, Paper number IMECE2004-60185, (2004)

Xu, J., and Fisher T. S., in *The Ninth Intersociety Conference on Thermal and Thermomechanical Phenomena in Electronic Systems* 2 , 549 (2004).

Yang, R.; Chen, G., "Thermal conductivity modeling of periodic two-dimensional nanocomposites," *Phys. Rev. B. 69*, 195316 (2004).

Ziman, J.,**.** Electrons and Phonons; The Theory of Transport Phenomena in Solids (Oxford, Clarendon Press 1960).

Zou, J., and Alexander, B., "Phonon Heat Conduction in A Semiconductor Nanowire," *J. Appl. Phys.* 89, 2932 (2001).

Vita

Sanjoy Kumar Saha was born in Kolkata, West Bengal, India on June 16th, 1978., the son of Sachindra Nath Saha and Tulsi Rani Saha. He did his schooling at Laban Hrad Vidyapith and St. Xavier's College. After that he joined Indian Institute of Technology, Kharagpur, India and received Bachelor of Science (Hons.) degree in Mechanical Engineering in July 2000. He joined Telco, India as a Mechanical Engineer and worked for one year. After that he joined Arizona State University and received M.S. degree in Mechanical Engineering in August 2003. In August 2003 he joined the graduate school of University of Texas at Austin for his Ph.D. degree. During 2005 summer and fall he worked as research intern at Nanocoolers, Inc, Austin, TX. During 2006 summer he interned at AMD, Austin, TX. Currently he is working full time at Dell, Austin, TX. He married Shawli Sengupta in January 2003.

Permanent address: BL-181, Sector 2, Saltlake, Kolkata, West Bengal, India, Pin-700091

This dissertation was typed by the author.